

# High-order strongly nonlinear long wave approximation and solitary wave solution

Wooyoung Choi<sup>†</sup>

Department of Mathematical Sciences, New Jersey Institute of Technology, Newark, NJ 07102-1982, USA

(Received 10 February 2022; revised 14 May 2022; accepted 20 June 2022)

We consider high-order strongly nonlinear long wave models expanded in a single small parameter measuring the ratio of the water depth to the characteristic wavelength. By examining its dispersion relation, the high-order system for the bottom velocity is found stable to all disturbances at any order of approximation. On the other hand, systems for other velocities can be unstable and even ill-posed, as signified by the unbounded maximum growth. Under the steady assumption, a new third-order solitary wave solution of the Euler equations is obtained using the high-order strongly nonlinear system and is expanded in an amplitude parameter, which is different from that used in weakly nonlinear theory. The third-order solution is shown to well describe various physical quantities induced by a finite-amplitude solitary wave, including the wave profile, horizontal velocity profile, particle velocity at the crest and bottom pressure. For numerical computations, the first- and second-order strongly nonlinear systems for the bottom velocity are considered. It is shown that finite difference schemes are unstable due to truncation errors introduced in approximating high-order spatial derivatives and, therefore, a more accurate spatial discretization scheme is necessary. Using a pseudo-spectral method based on finite Fourier series combined with an iterative scheme for the inversion of a non-local operator, the strongly nonlinear systems are solved numerically for the propagation of a single solitary wave and the head-on collision of two counter-propagating solitary waves of finite amplitudes, and the results are compared with previous laboratory measurements.

**Key words:** solitary waves, surface gravity waves

## 1. Introduction

Nonlinear surface gravity waves in shallow water have been studied using various mathematical models derived under the long wave assumption that the water depth  $h$  is much smaller than the characteristic wavelength  $\lambda$ , or, equivalently, the dispersion parameter  $\beta$  defined by  $\beta = h/\lambda$  is small. In addition, the nonlinearity parameter  $\alpha$  defined

<sup>†</sup> Email address for correspondence: [wychoi@njit.edu](mailto:wychoi@njit.edu)

by  $\alpha = a/h$ , with  $a$  being the wave amplitude, has been introduced and plays a crucial role in characterizing the long models.

Assuming the balance between dispersion and nonlinearity, or  $\alpha = O(\beta^2) \ll 1$ , a number of weakly nonlinear long wave models have been obtained from the Euler equations, and their solitary wave solutions have been studied extensively. The most well-known models include the Boussinesq equations and the Korteweg–de Vries (KdV) equation for bi- and uni-directional waves, respectively. These models have been improved extensively, including higher-order nonlinear and dispersive terms, for a wide range of applications; see, e.g. an earlier review by Miles (1980). A similar asymptotic technique with  $\alpha = O(\beta^2) \ll 1$  has also been applied to the steady Euler equations to find explicit asymptotic solitary wave solutions, for example, correct to the third order in  $\alpha$  by Grimshaw (1971) and to the ninth order by Fenton (1972).

While  $\beta \ll 1$  should be assumed for long waves, the smallness assumption on  $\alpha$  can be removed to obtain another class of nonlinear long wave models. Such models were derived by Su & Gardner (1969) and Green & Naghdi (1976) for one- and two-dimensional waves, respectively, and describe the time evolution of the surface elevation and the depth-averaged horizontal velocity field. The Su–Gardner or Green–Naghdi (SG/GN) equations are the shallow water equations with leading-order dispersive terms that appear at  $O(\beta^2)$ . As no explicit assumption on the magnitude of  $\alpha$  was made, the SG/GN equations can be considered a strongly nonlinear long wave model characterized by nonlinear dispersive terms. When the dispersive terms are linearized, the SG/GN equations can be reduced to the weakly nonlinear Boussinesq equations.

Interestingly, for the steady case, the asymptotic assumption of  $\alpha = O(1)$  and  $\beta \ll 1$  was adopted by Rayleigh (1876) more than a century ago. In fact, the ordinary differential equation for solitary waves that Rayleigh (1876) studied is exactly the travelling-wave limit of the SG/GN equations. Therefore, Rayleigh's solution is the solitary wave solution of the SG/GN model. Almost 80 years later, Rayleigh's equation was rediscovered by Serre (1953).

Similarly to weakly nonlinear models, the SG/GN equations were also modified to improve their dispersive relation for short waves that are often excited in many applications. Nwogu (1993) proposed to use the horizontal velocity at an intermediate depth, instead of the depth-averaged velocity, for the weakly nonlinear Boussinesq equations to better compare their linear dispersion relation with that of the linearized Euler equations. Using this idea, a strongly nonlinear long wave model for the velocity at an intermediate depth was obtained by Wei *et al.* (1995), who studied numerically the propagation of solitary waves over bottom topography and showed that their numerical solutions are in good agreement with the numerical solutions of the Euler equations until the wave slope becomes too high.

To better describe finite-amplitude long waves, these strongly nonlinear models have been also extended to include terms of  $O(\beta^4)$  or higher. A series of such efforts have been made by Wu (1998, 1999), Madsen & Schäffer (1998), Agnon, Madsen & Schäffer (1999), Madsen, Bingham & Liu (2002) and many others. In particular, Wu (1998) presented a systematic approach to find strongly nonlinear long wave models for different fluid velocities, including the depth-averaged velocity, the bottom velocity, the surface velocity and the velocity at an intermediate depth. Among these, the strongly nonlinear models for the surface velocity and depth-averaged velocity are known to preserve the original Hamiltonian structure of the Euler equations even if they are truncated at an arbitrary order of  $\beta^2$  (Zakharov 1968; Matsuno 2015). This is, however, true only in an asymptotic sense for the systems for other velocities.

While these high-order strongly nonlinear models are expected to better describe the evolution of finite-amplitude long waves, they need to be used with care for applications as their solution behaviour has not been fully understood. For example, when truncated at  $O(\beta^4)$ , the system for the depth-averaged velocity is ill-posed (Matsuno 2016) and its initial value problem cannot be solved numerically without any artificial filter to remove short-wavelength disturbances that grow extremely fast. Here the ill posedness refers to the case when the growth rate of unstable disturbances increases without bound as not only  $k \rightarrow \infty$ , but also  $k$  approaches a critical wavenumber above which the system is unstable. Similar observations of unstable short-wavelength disturbances have been made when the long wave models for other velocities are solved numerically (Kirby 2020; Madsen & Fuhrman 2020). A main source of the difficulty observed in previous studies could be from the ill posedness of these long wave models (Choi 2019), as well as numerical errors introduced when high-order spatial derivatives are evaluated.

In this paper, we study both analytically and numerically a high-order strongly nonlinear long wave model for the bottom velocity expanded in  $\beta^2$ , which can be shown to be well-posed at any order of approximation. While the choice of a well-posed model is essential for applications, there is no guarantee that the model remains well behaved when it is numerically approximated. This is even more true for a strongly nonlinear model that contains high-order nonlinear dispersive terms with high-order spatial derivatives. Here, we consider both finite difference and pseudo-spectral methods and propose a stable numerical scheme to solve the strongly nonlinear models.

This paper is organized as follows. After examining the ill posedness of truncated linearized long wave models in § 2, we present the two-dimensional strongly nonlinear long wave model for the bottom velocity in § 3, from which the third-order solitary wave solution of the Euler equations is obtained in § 4. After its relationship with other long wave models is discussed in § 5, the model is solved numerically for the propagation of solitary waves and the head-on collision of two counter-propagating solitary waves in § 6. Concluding remarks are given in § 7.

## 2. Basic formulation for nonlinear long waves

For water waves propagating in two horizontal dimensions, the free surface boundary conditions can be written (Zakharov 1968) as

$$\zeta_t + \nabla\Phi \cdot \nabla\zeta = (1 + |\nabla\zeta|^2)W, \quad \Phi_t + \frac{1}{2}|\nabla\Phi|^2 + g\zeta = \frac{1}{2}(1 + |\nabla\zeta|^2)W^2, \quad (2.1a,b)$$

where  $\zeta(\mathbf{x}, t)$  is the surface elevation,  $\Phi(\mathbf{x}, t) = \phi(\mathbf{x}, z = \zeta, t)$  is the velocity potential evaluated at the free surface,  $W$  is the vertical velocity evaluated at the free surface defined by  $W = \phi_z|_{z=\zeta}$  and  $g$  is the gravitational acceleration. Here, the subscripts  $t$  and  $z$  represent partial differentiations with respect to time  $t$  and the vertical coordinate  $z$ , respectively, and  $\nabla$  is the two-dimensional horizontal gradient given by  $\nabla = (\partial/\partial x, \partial/\partial y)$ . These equations can be regarded as a system of nonlinear evolution equations for  $\zeta$  and  $\Phi$  once  $W$  is expressed in terms of these two variables.

### 2.1. Linear models

For small-amplitude waves, the system given by (2.1) can be linearized to

$$\zeta_t = W, \quad \Phi_t + g\zeta = 0. \quad (2.2a,b)$$

In the meantime,  $\Phi$  and  $W$  can be approximated by those evaluated at the mean free surface ( $z = 0$ ) so that  $\Phi \simeq \phi(\mathbf{x}, 0, t) = \phi_0(\mathbf{x}, t)$  and  $W \simeq \phi_z(\mathbf{x}, 0, t) = w_0(\mathbf{x}, t)$ .

When the three-dimensional Laplace equation is solved for  $\phi$  imposing the bottom boundary condition given by  $\partial\phi/\partial z|_{z=-h} = 0$ , its solution can be written, in Fourier space, as

$$\hat{\phi}(\mathbf{k}, z, t) = \{\cosh[k(z + h)]/\cosh(kh)\}\hat{\phi}_0(\mathbf{k}, t), \tag{2.3}$$

where  $\hat{f}(\mathbf{k}, z, t)$  is the Fourier transform of  $f(\mathbf{x}, z, t)$ ,  $k = |\mathbf{k}|$  with  $\mathbf{k}$  being the two-dimensional wavenumber vector and  $h$  is the constant water depth. Then, from (2.3), one can obtain

$$\hat{w}_0(\mathbf{k}, t) = (k \tanh kh)\hat{\phi}_0(\mathbf{k}, t), \tag{2.4}$$

from which the approximate expression for  $W$  is given, in terms of  $\Phi$ , by

$$\hat{W}(\mathbf{k}, t) \simeq (k \tanh kh)\hat{\Phi}(\mathbf{k}, t). \tag{2.5}$$

Finally, after taking the Fourier transform of (2.2) and using (2.5), the linear evolution equations for  $\zeta$  and  $\Phi$  can be written, in Fourier space, as

$$\hat{\zeta}_t = (k \tanh kh)\hat{\Phi}, \quad \hat{\Phi}_t + g\hat{\zeta} = 0. \tag{2.6a,b}$$

For  $(\hat{\zeta}, \hat{\Phi}) \sim \exp(-i\omega t)$ , (2.6) yields the full linear dispersion relation for surface gravity waves given by

$$\omega^2 = gk \tanh kh, \tag{2.7}$$

from which one can see that the wave frequency  $\omega$  is always real as  $k > 0$ .

For long waves ( $kh \ll 1$ ),  $\mathcal{T} = \tanh kh$  can be expanded as

$$\mathcal{T} = \sum_{n=0}^{\infty} \frac{2^{2n+2}(2^{2n+2} - 1)B_{2n+2}}{(2n + 2)!} (kh)^{2n+1}, \tag{2.8}$$

where  $B_{2n}$  are the Bernoulli numbers given by  $B_0 = 1, B_2 = 1/6, B_4 = -1/30, B_6 = 1/42, \dots$ . This infinite series converges to  $\tanh kh$  as long as  $kh < \pi/2$  (due to singularities at  $kh = \pm i(\pi/2)$  in the complex  $k$ -plane), but, when it is approximated for long waves, its behaviour depends sensitively on how it is truncated.

When the upper limit for the summation in (2.8) is replaced by an integer  $M(\geq 0)$ , the truncated linear system (2.6) is given by

$$\hat{\zeta}_t = k\mathcal{T}_M \hat{\Phi}, \quad \hat{\Phi}_t + g\hat{\zeta} = 0, \tag{2.9a,b}$$

where  $\mathcal{T}_M$  represents the  $M$ th-order long wave approximation of  $\mathcal{T}$  valid to  $O(\beta^{2M})$  as  $kh = O(\beta)$ . The linear dispersion relation of this truncated system is then given by

$$\omega^2 \simeq ghk^2 \left[ 1 - \frac{1}{3}(kh)^2 + \frac{2}{15}(kh)^4 + \dots + \frac{2^{2M+2}(2^{2M+2} - 1)B_{2M+2}}{(2M + 2)!} (kh)^{2M} \right]. \tag{2.10}$$

Now one can see that, if  $M$  is an odd integer, the right-hand side of (2.10) becomes negative for large  $k$  so that  $\omega$  becomes purely imaginary. As the imaginary part of  $\omega$ , or the growth rate is proportional to  $k^{M+1}$ , it increases without bound as  $k \rightarrow \infty$  and, therefore, the truncated system with odd  $M$  is ill-posed. For example, as shown in figure 1(a), short-wavelength disturbances of  $kh \gtrsim 1.732$  and  $kh \gtrsim 1.647$  are unstable with the growth rates proportional to  $k^2$  and  $k^4$  for  $M = 1$  and 3, respectively. Under the linear assumption, as the free surface velocity potential  $\Phi$  can be approximated by the mean level velocity potential  $\phi_0$ , this discussion is parallel to that for the long wave model for  $\phi_0$  in Madsen & Schäffer (1998).

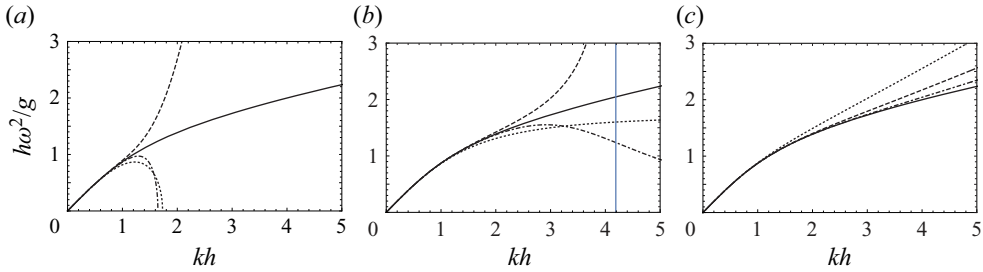


Figure 1. Linear dispersion relations between the wave frequency  $\omega$  and the wavenumber  $k$  for the systems for (a) the surface potential; (b) the depth-averaged velocity; (c) the bottom potential given by (2.10), (2.13) and (2.16), respectively. Three different approximations (dotted:  $M = 1$ ; dashed:  $M = 2$ ; dash-dotted:  $M = 3$ ) are compared with the full dispersion relation of the linearized Euler equations (solid) given by (2.7). The vertical line in (b) shows the value of  $k_c$ , where a singularity appears for  $M = 2$ .

If  $M$  is an even integer, the wave frequency  $\omega$  is always real, but  $\omega \sim k^{M+1}$  increases rapidly with  $k$ . This requires one to use a very small time step when the system for  $\zeta$  and  $\Phi$  is solved numerically as the criterion for numerical stability for a time integration scheme can be written as  $\omega\Delta t \leq C$ , with  $C$  being a constant depending on the scheme. Therefore, the long wave model for the surface variables ( $\zeta$  and  $\Phi$ ) with any  $M$  might be inappropriate for numerical computations.

Instead of the surface velocity potential  $\Phi$ , the well-known Boussinesq equations are often written in terms of the depth-averaged velocity defined by

$$\bar{\mathbf{u}} = \frac{1}{(h + \zeta)} \int_{-h}^{\zeta} \nabla\phi \, dz. \tag{2.11}$$

For small-amplitude waves, after replacing the upper limit of the integration by 0 and using (2.3), the Fourier transform of  $\bar{\mathbf{u}}$  can be approximated by  $\hat{\bar{\mathbf{u}}} \simeq -ik\{\tanh kh/(kh)\}\hat{\Phi}$ , from which we have  $h\widehat{\nabla \cdot \bar{\mathbf{u}}} \simeq -(k \tanh kh)\hat{\Phi}$ . Then, from (2.9), the linear system for  $\zeta$  and  $\bar{\mathbf{u}}$  can be found, in Fourier space, as

$$\hat{\zeta}_t = -h\widehat{\nabla \cdot \bar{\mathbf{u}}}, \quad (kh \coth kh)\hat{\bar{\mathbf{u}}}_t + g\widehat{\nabla}\zeta = 0. \tag{2.12a,b}$$

For a long wave, when truncated at  $O(\beta^{2M})$ , the linear system (2.12) yields the following dispersion relation

$$\left[ 1 + \frac{1}{3}(kh)^2 - \frac{1}{45}(kh)^4 + \dots + \frac{2^{2M}B_{2M}}{(2M)!}(kh)^{2M} \right] \omega^2 \simeq ghk^2, \tag{2.13}$$

where the expansion on the left-hand side of (2.13) is the truncated Taylor series of  $kh \coth kh$ . Contrary to the system for the surface velocity potential  $\Phi$ , the system for the depth-averaged velocity is well-posed for odd  $M$ , but is problematic for even  $M$ . For example, for  $M = 2$ , the system is unstable for disturbances of  $k > k_c$  with  $k_c h = [(15 + 9\sqrt{5})/2]^{1/2} \simeq 4.191$ . Although the growth rate decreases to 0 as  $k \rightarrow \infty$ , there is a singularity at  $k = k_c$ , where the growth rate becomes infinity, as shown in figure 1(b). This implies that the depth-averaged system given by (2.12) with even  $M$  should be avoided (Matsuno 2016). On the other hand, for odd  $M$ , the wave frequency  $\omega$  is real and approaches zero as  $k$  increases, which is ideal for numerical stability, as discussed previously. Therefore, the depth-averaged system only with odd  $M$  would be useful for numerical computations.

Another variable often adopted for long wave models is the bottom velocity potential, or the bottom velocity. For small-amplitude waves,  $\Phi$  and the bottom velocity potential  $\phi_b(\mathbf{x}, t) = \phi(\mathbf{x}, -h, t)$  are related, from (2.3), as

$$\hat{\Phi} \simeq \hat{\phi}_0(\mathbf{k}, t) = (\cosh kh)\hat{\phi}_b(\mathbf{k}, t). \tag{2.14}$$

Then, the linear evolution equations for  $\hat{\zeta}$  and  $\hat{\phi}_b$  can be obtained, from (2.6) with (2.14), as

$$\hat{\zeta}_t = (k \sinh kh)\hat{\phi}_b, \quad (\cosh kh)\hat{\phi}_{bt} + g\hat{\zeta} = 0. \tag{2.15a,b}$$

For  $kh = O(\beta) \ll 1$ , when the expansions of  $\sinh kh$  and  $\cosh kh$  are truncated at  $O(\beta^M)$ , as before, the dispersion relation for (2.15) is given by

$$\left[ 1 + \frac{(kh)^2}{2!} + \dots + \frac{(kh)^{2M}}{(2M)!} \right] \omega^2 \simeq ghk^2 \left[ 1 + \frac{(kh)^2}{3!} + \dots + \frac{(kh)^{2M}}{(2M+1)!} \right], \tag{2.16}$$

from which one can see that  $\omega$  is real for any values of  $k$  and  $M$ . Unlike that for the surface velocity potential or the depth-averaged velocity, the system for the bottom velocity given by (2.15) is stable to all disturbances at any order of approximation and is therefore well-posed. As can be seen in figure 1(c), as  $M$  increases, the dispersion relation (2.16) converges uniformly to the full linear dispersion relation given by (2.7).

Following Nwogu (1993), the long wave model can be expressed in terms of the velocity potential at an arbitrary vertical level  $z = z_\alpha$  ( $-h \leq z_\alpha \leq 0$ ), which can be related to the bottom variable as

$$\hat{\phi}_b(\mathbf{k}, t) = \operatorname{sech}[k(z_\alpha + h)]\hat{\phi}_\alpha(\mathbf{k}, t). \tag{2.17}$$

By substituting this into (2.15), the linear system for  $\zeta$  and  $\phi_\alpha$  is obtained as

$$\hat{\zeta}_t = (k \sinh kh) \operatorname{sech}[k(z_\alpha + h)]\hat{\phi}_\alpha, \quad (\cosh kh) \operatorname{sech}[k(z_\alpha + h)]\hat{\phi}_{\alpha t} + g\hat{\zeta} = 0. \tag{2.18a,b}$$

When the linear system is truncated at  $O(\beta^M)$ , its dispersion relation can be found as

$$\omega^2 = ghk^2 \left[ \sum_{n=0}^M a_{2n}(kh)^{2n} \right] / \left[ \sum_{n=0}^M b_{2n}(kh)^{2n} \right], \tag{2.19}$$

where  $a_{2n}$  and  $b_{2n}$  are given by

$$a_{2n} = \sum_{j=0}^n \frac{E_{2j}}{(2(n-j)+1)!(2j)!} \left(1 + \frac{z_\alpha}{h}\right)^{2j}, \quad b_{2n} = \sum_{j=0}^n \frac{E_{2j}}{(2(n-j))!(2j)!} \left(1 + \frac{z_\alpha}{h}\right)^{2j}, \tag{2.20a,b}$$

with  $E_n$  being the  $n$ th Euler number given by  $E_0 = 1, E_2 = -1, E_4 = 5, E_6 = -61, \dots$ . For example, for  $M = 2$ , we have

$$\omega^2 = ghk^2 \left[ \frac{1 + \frac{1}{2} \left\{ \frac{1}{3} - \left(1 + \frac{z_\alpha}{h}\right)^2 \right\} (kh)^2 + \frac{1}{12} \left\{ \frac{1}{10} - \left(1 + \frac{z_\alpha}{h}\right)^2 + \frac{5}{2} \left(1 + \frac{z_\alpha}{h}\right)^4 \right\} (kh)^4}{1 + \frac{1}{2} \left\{ 1 - \left(1 + \frac{z_\alpha}{h}\right)^2 \right\} (kh)^2 + \frac{1}{4} \left\{ \frac{1}{6} - \left(1 + \frac{z_\alpha}{h}\right)^2 + \frac{5}{6} \left(1 + \frac{z_\alpha}{h}\right)^4 \right\} (kh)^4} \right]. \tag{2.21}$$

When the second-order dispersive terms proportional to  $(kh)^4$  are neglected, this is identical to the dispersion relation obtained by Nwogu (1993). For  $z_\alpha = 0$  and  $z_\alpha = -h$ , (2.21) can be reduced to (2.13) and (2.16) with  $M = 2$ , respectively.

As discussed previously, when the linear system (2.18) is truncated, its ill posedness is determined by the behaviour of large  $k$  disturbances, or, equivalently, the sign of  $a_{2M}/b_{2M}$  in (2.19). For example, for  $M = 1$ , the large- $k$  disturbances is stable only when  $-1 \leq z_\alpha/h \leq -1 + 1/\sqrt{3} \simeq -0.423$  and  $z_\alpha$  should be chosen in this range. For an arbitrary value of  $M$ , one should find a range of  $z_\alpha$  for which the sign of  $a_{2M}/b_{2M}$  is always positive. For example, for  $M = 2$  and  $M = 3$ , the conditions for stability are given by  $-1 \leq z_\alpha/h \leq -1 + 1/\sqrt{5} \simeq -0.553$  and  $-1 \leq z_\alpha/h \lesssim -0.499$ , respectively. While it fluctuates with  $M$ , the permissible range of  $z_\alpha$  is small and close to the bottom as  $M$  increases. Therefore, it is ideal to choose the system for the bottom velocity potential or velocity for applications as it is well-posed at any order of approximation.

It should be mentioned that our main goal is not to improve the dispersion relation for short waves, but to develop a well-posed strongly nonlinear long wave system, although it would be desirable to improve the dispersive behaviour of short waves. A system with the full linear dispersion relation for water waves will be discussed in § 5.3.

### 2.2. Nonlinear models

Here, we sketch briefly the derivation of strongly nonlinear long wave models. To close (2.1),  $W$  needs to be expressed in terms of  $\zeta$  and  $\Phi$  for the system for the surface potential while  $W$  and  $\Phi$  need to be written, for example, in terms of  $\zeta$  and  $\phi_b$  for the system for the bottom potential.

First the three-dimensional velocity potential  $\phi(\mathbf{x}, z, t)$  is expanded in Taylor series about a fixed vertical level, or  $z = z_\alpha$

$$\begin{aligned} \phi(\mathbf{x}, z, t) &= \sum_{j=0}^{\infty} \frac{(-1)^j (z - z_\alpha)^{2j}}{(2j)!} \nabla^{2j} \phi|_{z=z_\alpha} \\ &+ \sum_{j=0}^{\infty} \frac{(-1)^j (z - z_\alpha)^{2j+1}}{(2j+1)!} \nabla^{2j+1} \cdot \nabla^{-1} \frac{\partial \phi}{\partial z} \Big|_{z=z_\alpha}. \end{aligned} \quad (2.22)$$

By introducing in (2.22)

$$\phi_\alpha = \phi|_{z=z_\alpha}, \quad w_\alpha = \partial \phi / \partial z|_{z=z_\alpha}, \quad (2.23a,b)$$

$\phi(\mathbf{x}, z, t)$  and  $w(\mathbf{x}, z, t) = \partial \phi / \partial z$  can be written (Madsen *et al.* 2002; Madsen & Agnon 2003) as

$$\phi = \cos[(z - z_\alpha)\nabla] \phi_\alpha + \sin[(z - z_\alpha)\nabla] \cdot \nabla^{-1} w_\alpha, \quad (2.24a)$$

$$w = -\sin[(z - z_\alpha)\nabla] \cdot \nabla \phi_\alpha + \cos[(z - z_\alpha)\nabla] w_\alpha. \quad (2.24b)$$

When  $\phi$  and  $w$  in (2.24) are evaluated at  $z = \zeta$ , the expressions for the free surface variables  $\Phi(\mathbf{x}, t)$  and  $W(\mathbf{x}, t)$  can be found, in terms of  $\phi_\alpha$  and  $w_\alpha$ , as

$$\Phi = \cos[(\zeta - z_\alpha)\nabla] \phi_\alpha + \sin[(\zeta - z_\alpha)\nabla] \cdot \nabla^{-1} w_\alpha, \quad (2.25a)$$

$$W = -\sin[(\zeta - z_\alpha)\nabla] \cdot \nabla \phi_\alpha + \cos[(\zeta - z_\alpha)\nabla] w_\alpha. \quad (2.25b)$$

Depending on the choice of  $z_\alpha$ , different nonlinear wave models can be obtained. For example, in the high-order spectral (HOS) method for surface waves on finite-depth water (Dommermuth & Yue 1987; West *et al.* 1987; Craig & Sulem 1993),  $z_\alpha = 0$

is chosen. After using the relationship between  $w_0$  and  $\phi_0$  given by (2.4), the expression for  $W$  in infinite series can be found, in terms of  $\zeta$  and  $\Phi$ , from (2.25) (Choi 2019). For numerical computations, one should truncate the series to a certain order in wave steepness defined by  $\epsilon = a/\lambda \ll 1$  and the resulting truncated system for  $\zeta$  and  $\Phi$  can be considered an asymptotic model for weakly nonlinear waves in water of finite depth.

For finite-amplitude long waves in shallow water, it is more appropriate to choose  $z_\alpha = -h$  to rewrite (2.24), with  $w_\alpha = 0$  at the (flat) bottom, as

$$\phi(\mathbf{x}, z, t) = \cos[(z + h)\nabla]\phi_b, \quad w(\mathbf{x}, z, t) = -\sin[(z + h)\nabla]\cdot\nabla\phi_b, \quad (2.26a,b)$$

where  $\phi_b(\mathbf{x}, t)$  is the bottom velocity potential, as before. By substituting  $z = \zeta$  into (2.26),  $\Phi$  and  $W$  can be expressed, in terms of  $\zeta$  and  $\phi_b$ , as

$$\Phi = \cos[(\zeta + h)\nabla]\phi_b, \quad W = -\sin[(\zeta + h)\nabla]\cdot\nabla\phi_b. \quad (2.27a,b)$$

Then, substituting (2.27) into (2.1) yields formally a system of nonlinear evolution equations for  $\zeta$  and  $\phi_b$  although the cosine and sine functions in (2.27) need to be expanded in infinite series and then truncated for numerical evaluations. As will be seen in § 3, the truncated system is equivalent to an asymptotic model valid for small  $\beta$ . Detailed discussions on the system for  $\zeta$  and  $\phi_b$  will be presented in § 3.

Similarly, one can find a system for  $\phi_\alpha$  using its relationship with  $\phi_b$  given, from (2.6a), by  $\phi_\alpha = \cos[(z_\alpha + h)\nabla]\phi_b$ . After its inversion for the expression for  $\phi_b$  is substituted into (2.27) to find the expressions for  $\Phi$  and  $W$  in terms of  $\zeta$  and  $\phi_\alpha$ , a closed system for  $\zeta$  and  $\phi_\alpha$  can be found from (2.1). As shown in Choi (2019), one can also find a system for  $\zeta$  and  $\Phi$  from (2.1) by using the expression for  $W$  in terms of  $\zeta$  and  $\Phi$  found from (2.27). As discussed in § 2.1, depending on the order of approximation, the system for  $(\zeta, \phi_\alpha)$  or  $(\zeta, \Phi)$  can be ill-posed and will not be further considered. Instead, we will hereinafter focus on the nonlinear system for  $(\zeta, \phi_b)$ , which is well-posed at any order of approximation.

### 3. High-order long wave model for the bottom potential

#### 3.1. Expansion in terms of the bottom velocity potential

By expanding the cosine and sine functions in (2.27),  $\Phi$  and  $W$  can be expressed, in terms of  $\zeta$  and  $\phi_b$ , as

$$\Phi = \sum_{m=0}^{\infty} \Phi_{2m}, \quad \Phi_{2m} = \frac{(-1)^m}{(2m)!} \eta^{2m} \nabla^{2m} \phi_b, \quad (3.1a,b)$$

$$W = \sum_{m=0}^{\infty} W_{2m}, \quad W_{2m} = \frac{(-1)^{m+1}}{(2m+1)!} \eta^{2m+1} \nabla^{2(m+1)} \phi_b, \quad (3.2a,b)$$

where  $\eta = h + \zeta$ , and both  $\Phi_{2m}$  and  $W_{2m}$  explicitly depend only on  $\zeta$  and  $\phi_b$ . Assuming that  $\eta\nabla = O(h/\lambda) = O(\beta) \ll 1$  with  $\zeta/h = O(a/h) = O(\alpha) = O(1)$ , one can notice that  $\Phi_{2m}/\Phi = O(\beta^{2m})$  and  $W_{2m}/|\nabla\Phi| = O(\beta^{2m+1})$  for  $m \geq 0$ . Although no small parameter is explicitly introduced, these series can be considered asymptotic series in  $\beta^2$  when truncated.



## High-order long wave approximation

### 3.2. System of nonlinear evolution equations

By substituting (3.1) and (3.2) into (2.1), the nonlinear evolution equations for  $\zeta$  and  $\phi_b$  can be obtained as

$$\zeta_t = \sum_{m=0}^{\infty} Q_{2m}(\zeta, \phi_b), \quad \Phi_t = \sum_{m=0}^{\infty} R_{2m}(\zeta, \phi_b), \quad (3.3a,b)$$

where  $\Phi$  is given, in terms of  $\zeta$  and  $\phi_b$ , by (3.1). In (3.3),  $Q_{2m}$  ( $m \geq 0$ ) are given by

$$Q_0 = -\nabla\zeta \cdot \nabla\Phi_0 + W_0, \quad Q_{2m} = -\nabla\zeta \cdot \nabla\Phi_{2m} + W_{2m} + |\nabla\zeta|^2 W_{2(m-1)} \quad \text{for } m \geq 1, \quad (3.4a,b)$$

while  $R_{2m}$  ( $m \geq 0$ ) are given by

$$\begin{aligned} R_0 &= -g\zeta - \frac{1}{2}|\nabla\Phi_0|^2, \quad R_2 = -\nabla\Phi_0 \cdot \nabla\Phi_2 + \frac{1}{2}W_0^2, \quad (3.5a,b) \\ R_{2m} &= -\frac{1}{2} \sum_{j=0}^m \nabla\Phi_{2j} \cdot \nabla\Phi_{2(m-j)} + \frac{1}{2} \sum_{j=0}^{m-1} W_{2j} W_{2(m-j-1)} \\ &\quad + \frac{1}{2} |\nabla\zeta|^2 \sum_{j=0}^{m-2} W_{2j} W_{2(m-j-2)} \quad \text{for } m \geq 2. \quad (3.5c) \end{aligned}$$

When the expressions for  $\Phi_{2m}$  and  $W_{2m}$  given by (3.1) and (3.2) are substituted into (3.4) and (3.5), one can find the explicit expressions of  $Q_{2m}$  and  $R_{2m}$ . In particular, it is useful to notice that  $Q_{2m}$  can be re-written as

$$Q_{2m} = \nabla \cdot \left[ \frac{(-1)^{m+1}}{(2m+1)!} \eta^{2m+1} \nabla^{2m} \nabla \phi_b \right] \quad \text{for } m \geq 0. \quad (3.6)$$

As (3.3b) is the evolution equation for  $\Phi$ , an additional step is necessary to find  $\phi_b$  from  $\Phi$ . When the infinite series for  $\Phi$  in (3.1) is inverted,  $\phi_b$  can be expressed, in terms of  $\zeta$  and  $\Phi$ , as

$$\phi_b = \sum_{m=0}^{\infty} \phi_{2m}^b \quad \phi_0^b = \Phi, \quad \phi_{2m}^b = \sum_{j=1}^m \frac{(-1)^{j+1}}{(2j)!} \eta^{2j} \nabla^{2j} \phi_{2(m-j)}^b \quad \text{for } m \geq 1. \quad (3.7a-c)$$

To be discussed in § 5, for numerical computations, one needs to truncate the right-hand sides of (3.3) to a desired order of  $\beta^2$ . As both  $Q_{2m}$  and  $R_{2m}$  are  $O(\beta^{2m})$  for  $m \geq 0$ , the system truncated to  $m = M$  is asymptotically correct to  $O(\beta^{2M})$ .

### 3.3. Relation to the system for the depth-averaged velocity

By substituting (2.6a) into (2.11), the depth-averaged velocity  $\bar{\mathbf{u}}$  can be written, in terms of  $\zeta$  and  $\phi_b$ , as

$$\bar{\mathbf{u}} = \frac{1}{\eta} \sin(\eta \nabla) \phi_b = \sum_{m=0}^{\infty} \frac{(-1)^m}{(2m+1)!} \eta^{2m} \nabla^{2m} \mathbf{v}, \quad (3.8)$$

where  $\mathbf{v}$  is the bottom velocity given by

$$\mathbf{v} = \nabla \phi_b. \quad (3.9)$$

From (3.5c) and (3.8), one can see that the evolution equation for  $\zeta$  given by (3.3a) can be written as

$$\zeta_t + \nabla \cdot (\eta \bar{\mathbf{u}}) = 0, \tag{3.10}$$

which represents the exact conservation law of mass.

By inverting (3.8), the expression for  $\mathbf{v}$  can be found, in terms of  $\zeta$  and  $\bar{\mathbf{u}}$ , as

$$\mathbf{v} = \sum_{m=0}^{\infty} \bar{\mathbf{v}}_{2m}, \quad \bar{\mathbf{v}}_0 = \bar{\mathbf{u}}, \quad \bar{\mathbf{v}}_{2m} = \sum_{j=1}^m \frac{(-1)^{j+1}}{(2j+1)!} \eta^{2j} \nabla^{2j} \bar{\mathbf{v}}_{2(m-j)} \quad \text{for } m \geq 1. \tag{3.11a-c}$$

When this is substituted into (3.3b), the evolution equation for the depth-averaged velocity  $\bar{\mathbf{u}}$  can be found, as shown in Appendix A. As mentioned previously, the system for the depth  $\zeta$  and  $\bar{\mathbf{u}}$  are ill-posed when the order of approximation is even.

While the original three-dimensional velocity field is irrotational, the two-dimensional depth-averaged velocity field  $\bar{\mathbf{u}}$  is no longer irrotational. By taking the curl of (3.11) and using the irrotationality of  $\mathbf{v}$  ( $\nabla \times \mathbf{v} = \nabla \times \nabla \phi_b = 0$ ), the vorticity for the depth-averaged velocity given by

$$\nabla \times \bar{\mathbf{u}} = - \sum_{m=1}^{\infty} \nabla \times \bar{\mathbf{v}}_{2m}, \tag{3.12}$$

is non-zero although it is still weak for long waves as  $\bar{\mathbf{v}}_{2m} = O(\beta^{2m})$  for  $m \geq 1$ .

### 3.4. Conservation of energy

Zakharov (1968) showed that the system given by (2.1) can be written as Hamilton's equations

$$\zeta_t = \frac{\delta E}{\delta \Phi}, \quad \Phi_t = - \frac{\delta E}{\delta \zeta}, \tag{3.13a,b}$$

where  $\delta E / \delta \zeta$  and  $\delta E / \delta \Phi$  represent the functional derivatives of  $E$  with respect to  $\zeta$  and  $\Phi$ , respectively. Then the system (3.13) conserves the total energy  $E$  given by

$$E = \frac{1}{2} \int (g\zeta^2 + \Phi \zeta_t) \, dx. \tag{3.14}$$

After substituting (3.1) for  $\Phi$  and (3.3a) with (3.5c) for  $\zeta_t$  into (3.14),  $E$  can be expanded as

$$E = \sum_{m=0}^{\infty} E_{2m}(\zeta, \phi_b). \tag{3.15}$$

Here,  $E_{2m} = O(\beta^{2m})$  for  $m \geq 0$  are given by

$$E_0 = \frac{1}{2} \int (g\zeta^2 + \eta \nabla \phi_b \cdot \nabla \phi_b) \, dx, \tag{3.16a}$$

$$E_{2m} = \frac{1}{2} \int (-1)^m \sum_{j=0}^m \left[ \frac{\eta^{2j+1} \nabla^{2j} (\nabla \phi_b) \cdot \nabla (\eta^{2(m-j)} \nabla^{2(m-j)} \phi_b)}{(2j+1)! (2(m-j))!} \right] \, dx. \tag{3.16b}$$

The total energy written in infinite series is conserved, but its truncated expression is not a conserved quantity for the corresponding truncated system for  $\zeta$  and  $\phi_b$ . The truncated total energy is conserved only asymptotically. On the other hand, the systems for  $(\zeta, \Phi)$  and  $(\zeta, \bar{\mathbf{u}})$  conserve the truncated total energy exactly at any order of approximation (Matsuno 2015).

### 4. Third-order solitary wave solution

Under the weakly nonlinear assumption ( $\alpha \ll 1$ ), the explicit solitary wave solution of the Euler equations was obtained to the third order in  $\alpha$  by Grimshaw (1971) and to the ninth order by Fenton (1972). For the strongly nonlinear case of  $\alpha = O(1)$ , the leading-order solution with an error of  $O(\beta^2)$  was obtained by Rayleigh (1876), but no explicit higher-order solution has been known although it was computed numerically using a steady long wave model in the hodograph plane by Murashige & Choi (2015). Here, assuming  $\alpha = O(1)$ , we obtain a third-order solution of the Euler equations using the system for  $\zeta$  and  $\phi_b$  given by (3.3).

#### 4.1. Wave profile

For one-dimensional waves, after introducing  $X = x - ct$  and integrating once with  $(\zeta, \phi_{bX}) \rightarrow 0$  at  $X \rightarrow \pm\infty$ , (3.3) with (3.5c) can be written, in terms of  $\zeta(X)$  and  $v(X) = \phi_{bX}$ , as

$$-c\zeta = \sum_{m=0}^{\infty} \frac{(-1)^{m+1}}{(2m+1)!} \eta^{2m+1} D^{2m}[v] \quad \text{for } m \geq 0, \tag{4.1}$$

where  $c$  is the solitary wave speed and  $D = d/dX$ . This can be inverted to have the expression for  $v$ , in terms of  $\zeta$ , as

$$v = \sum_{m=0}^{\infty} v_{2m}^s, \quad v_0^s = \frac{c\zeta}{\eta}, \quad v_{2m}^s = \sum_{j=1}^m \frac{(-1)^{j+1}}{(2j+1)!} \eta^{2j} D^{2j}[v_{2(m-j)}^s] \quad m \geq 1. \tag{4.2a-c}$$

Notice that this can be also obtained from (3.10), or  $\bar{u} = c\zeta/\eta$ , with (3.11).

Then, from (3.1) and (3.2), the new expressions for  $\Phi$  and  $W$  can be found, in terms of  $\zeta$ , as

$$\Phi = \sum_{m=0}^{\infty} \Phi_{2m}^s, \quad \Phi_{2m}^s = \sum_{j=0}^m \frac{(-1)^j}{(2j)!} \eta^{2j} D^{2j-1}[v_{2(m-j)}^s], \tag{4.3a,b}$$

$$W = \sum_{m=0}^{\infty} W_{2m}^s, \quad W_{2m}^s = \sum_{j=0}^m \frac{(-1)^{j+1}}{(2j+1)!} \eta^{2j+1} D^{2j+1}[v_{2(m-j)}^s]. \tag{4.4a,b}$$

By substituting these into the steady form of (3.3b), one can find an ordinary differential equation for  $\zeta(X)$  as

$$\sum_{m=0}^{\infty} F_{2m}(\zeta; c) = 0, \quad F_{2m}(\zeta; c) = cD[\Phi_{2m}^s] + R_{2m}^s, \tag{4.5a,b}$$

where  $R_{2m}^s$  are given, from (3.5), by

$$R_0^s = -g\zeta - \frac{1}{2}(D[\Phi_0^s])^2, \quad R_2^s = -(D[\Phi_0^s])(D[\Phi_2^s]) + \frac{1}{2}(W_0^s)^2, \tag{4.6a,b}$$

$$R_{2m}^s = -\frac{1}{2} \sum_{j=0}^m (D[\Phi_{2j}^s])(D[\Phi_{2(m-j)}^s]) + \frac{1}{2} \sum_{j=0}^{m-1} W_{2j}^s W_{2(m-j-1)}^s + \frac{1}{2} (D[\zeta])^2 \sum_{j=0}^{m-2} W_{2j}^s W_{2(m-j-2)}^s \quad \text{for } m \geq 2. \tag{4.6c}$$

In (4.5),  $F_{2m} = O(\beta^{2m})$  are explicit functions of  $\zeta$ , and their explicit expressions for  $m = 0, 1, 2, 3$  are given in Appendix B.

After multiplying by  $\zeta_X$ , (4.5) can be integrated once with respect to  $X$  to have the following nonlinear ordinary differential equation

$$\sum_{m=0}^{\infty} N_{2m}(\zeta; c) = 0, \quad N_{2m}(\zeta; c) = \int_{-\infty}^X F_{2m}(\zeta; c) \zeta_{X'} dX'. \tag{4.7a,b}$$

The explicit expressions for  $N_{2m}$  ( $m = 0, 1, 2, 3$ ) are given by

$$N_0(\zeta; c) = \frac{\zeta^2}{2\eta} (c^2 - g\eta), \tag{4.8a}$$

$$N_2(\zeta; c) = -\left(\frac{c^2 h^2}{6}\right) \frac{\zeta'^2}{\eta}, \tag{4.8b}$$

$$N_4(\zeta; c) = -\frac{c^2 h^2}{90\eta} (2\eta^2 \zeta' \zeta''' - \eta^2 \zeta''^2 + 2\eta \zeta'^2 \zeta'' - 12\zeta'^4), \tag{4.8c}$$

$$N_6(\zeta; c) = -\frac{c^2 h^2}{1890\eta} [4\eta^4 \zeta' \zeta^{(5)} - 4\eta^3 (\eta \zeta'' - 6\zeta'^2) \zeta^{(4)} + 2\eta^4 \zeta''^2 - 6\eta^2 \zeta' (11\zeta'^2 + 5\eta \zeta'') \zeta''' + 10\eta^3 \zeta'^3 - 75\eta^2 \zeta'^2 \zeta''^2 - 90\zeta'^4 \zeta'' + 220\zeta'^6], \tag{4.8d}$$

where  $\zeta^{(n)} = d^n \zeta / dX^n$  and we have imposed the zero boundary conditions for  $\zeta$  and its derivatives at infinities. Once again, as  $N_{2m} = O(\beta^{2m})$ , the infinite series in (4.7) can be truncated by replacing the upper limit of the summation by a desired order of approximation  $M$ .

The zeroth-order approximation to (4.7), or  $N_0(\zeta; c) = 0$ , yields a trivial solution,  $\zeta = 0$ , when the zero boundary conditions at infinities are imposed. This implies that  $N_0(\zeta; c) = O(\beta^2)$  and one should include the  $O(\beta^2)$ -terms to find a non-trivial solution of (4.7).

#### 4.1.1. First-order solution

The ordinary differential equation that appears at  $O(\beta^2)$  is given, from (4.7), by  $N_0(\zeta_0; c_0) + N_2(\zeta_0; c_0) = 0$ , or

$$\zeta_0'^2 = \left(\frac{3g}{c_0^2 h^2}\right) \zeta_0^2 \left[\frac{c_0^2}{g} - (h + \zeta_0)\right], \tag{4.9}$$

where  $\zeta_0$  will be referred to as the first-order solution. From  $\zeta_0' = 0$  at  $\zeta_0 = a$ , the leading-order wave speed  $c_0$  and the amplitude  $a$  are related as

$$c_0^2 = g(h + a). \tag{4.10}$$

The solitary wave solution of (4.9) can be found as

$$\zeta_0(X) = a \operatorname{sech}^2(k_s X), \tag{4.11}$$

where  $k_s$  is given by

$$(k_s h)^2 = \frac{3}{4} \left(\frac{a}{h + a}\right). \tag{4.12}$$

### High-order long wave approximation

This is the solution that Rayleigh (1876) obtained in his seminal work under the sole assumption of  $\beta^2 \ll 1$ . It should be mentioned that (4.11) is also the solitary wave solution of the SG/GN system (5.11).

As  $(k_s h)^2 = O(\beta^2) \ll 1$  has been assumed for long waves, (4.12) shows that  $\gamma$  defined by

$$\gamma = \frac{\alpha}{1 + \alpha} = O(\beta^2) \ll 1, \quad (4.13)$$

should be small, which is true only when  $\alpha \ll 1$ . This implies that, even for the strongly nonlinear waves, a balance between nonlinearity and dispersion is still required for a solitary wave solution to exist. However, the balance occurs between  $\beta^2$  and  $\gamma$ , instead of  $\beta^2$  and  $\alpha$  for weakly nonlinear waves. As shown in §4.1.3, the asymptotic solution expanded in  $\beta^2$ , or equivalently in  $\gamma$ , compares well with the Euler solutions over a wider range of wave amplitudes than that expanded in  $\alpha$ .

#### 4.1.2. Third-order solution

An asymptotically consistent higher-order solitary wave solution can be found from (4.7) by writing  $c$  and  $\zeta$  as

$$c = \sum_{m=0}^{\infty} c_{2m}, \quad \zeta = \sum_{m=0}^{\infty} \zeta_{2m}(X), \quad (4.14a,b)$$

where the leading-order solutions  $c_0$  and  $\zeta_0(X)$  are given by (4.10) and (4.11), respectively, and both  $c_{2m}$  and  $\zeta_{2m}$  have been assumed to be  $O(\beta^{2m})$ . By substituting (4.14) into (4.7) and collecting terms of  $O(\beta^{2m})$ , one can find an equation for  $\zeta_{2m}$  ( $m \geq 1$ ) as

$$f_1(X)\zeta'_{2m} + f_2(X)\zeta_{2m} = f_3(X)c_{2m} + F_{2m}(X). \quad (4.15)$$

Here,  $f_j(X)$  ( $j = 1, 2, 3$ ) depending on  $\zeta_0$  and  $c_0$  remain the same for any  $m$  while  $F_{2m}(X)$  is a function of  $\zeta_{2l}$  and  $c_{2l}$  for  $l = 0, 1, \dots, m - 1$ . Notice that  $f_j$  ( $j = 1, 2, 3, 4$ ) are known before (4.15) is solved for  $\zeta_{2m}$ . The solution of (4.15) is then given by

$$\zeta_{2m} = \frac{1}{f_0} \int_{-\infty}^X f_0 \left( \frac{f_3}{f_1} c_2 + \frac{F_{2m}}{f_1} \right) dX, \quad f_0(X) = \exp \left[ \int (f_2/f_1) dX \right], \quad (4.16a,b)$$

where we have assumed symmetric profiles for  $\zeta_{2m}$  with neglecting the homogenous solutions.

At  $O(\beta^2)$ , we can find the leading-order corrections to  $c_0$  and  $\zeta_0$  from (4.15) with  $f_j(X)$  ( $j = 1, 2, 3$ ) and  $F_{2m}$  given by

$$f_1 = -\frac{c_0^2 h^2}{3} \zeta_0', \quad f_2 = c_0^2 \zeta_0 - g h \zeta_0 - \frac{3}{2} g \zeta_0^2, \quad f_3 = \frac{c_0 h^2}{3} \zeta_0'^2 - c_0 \zeta_0^2, \quad F_2 = -\eta N_4(\zeta_0, c_0), \quad (4.17a-d)$$

for which the integrating factor  $f_0(X)$  is given by  $f_0(X) = \sinh(2k_s x) / \tanh^2(k_s X)$  with  $k_s$  being defined in (4.12). By eliminating terms proportional to  $x \operatorname{sech}^2(k_s x) \tanh^2(k_s x)$  in

(4.16) to avoid secular terms (Grimshaw 1971; Fenton 1972),  $c_2$  and  $\zeta_2(X)$  can be found as

$$\frac{c_2}{c_0} = \frac{\alpha}{10}\gamma, \tag{4.18}$$

$$\frac{\zeta_2}{h} = \frac{\alpha}{300} \left( a_{20}S^2 + \sum_{j=1}^3 a_{2j}S^{2j}T^2 \right) \gamma, \tag{4.19}$$

where  $S = \text{sech}(k_s X)$ ,  $T = \tanh(k_s X)$  and  $a_{2j}(j = 0, 1, 2, 3)$  are given by

$$a_{20} = 15(5 + 6\alpha + \alpha^2), \quad a_{21} = -(225 + 150\alpha + 167\alpha^2), \tag{4.20a}$$

$$a_{22} = -7\alpha(30 + 13\alpha), \quad a_{23} = 63\alpha^2. \tag{4.20b}$$

Notice that  $c_2$  and  $\zeta_2$  are proportional to  $\gamma = O(\beta^2)$ , as expected.

Similarly, at  $O(\beta^4)$ ,  $c_4$  and  $\zeta_4(X)$  that are proportional to  $\gamma^2$  can be found as

$$\frac{c_4}{c_0} = \frac{\alpha(40 + 21\alpha)}{1400}\gamma^2, \tag{4.21}$$

$$\frac{\zeta_4}{h} = \frac{\alpha}{22050000} \left( a_{40}S^2 + \sum_{j=1}^6 a_{4j}S^{2j}T^2 \right) \gamma^2, \tag{4.22}$$

where  $a_{4j}(j = 0, 1, \dots, 6)$  are given by

$$a_{40} = -1050(-1575 - 1455\alpha + 1709\alpha^2 + 1843\alpha^3 + 254\alpha^4), \tag{4.23a}$$

$$a_{41} = -2\alpha(9161775 + 4616055\alpha + 5599225\alpha^2 + 964278\alpha^3), \tag{4.23b}$$

$$a_{42} = -12403125 - 21895650\alpha - 24960330\alpha^2 + 15477950\alpha^3 + 3116512\alpha^4, \tag{4.23c}$$

$$a_{43} = -2\alpha(-8037225 + 37783755\alpha + 39163725\alpha^2 + 12100858\alpha^3), \tag{4.23d}$$

$$a_{44} = 10\alpha^2(14635350 + 10836195\alpha + 2676968\alpha^2), \tag{4.23e}$$

$$a_{45} = 70\alpha^3(134985 + 125131\alpha), \tag{4.23f}$$

$$a_{46} = -4469535\alpha^4. \tag{4.23g}$$

To summarize, the third-order solitary wave solution valid to  $O(\beta^4)$ , or  $O(\gamma^2)$ , is given, from (4.10) and (4.11), (4.18) and (4.19), and (4.21) and (4.22), by

$$c = c_0 \left[ 1 + \frac{\alpha}{10}\gamma + \frac{\alpha(21\alpha + 40)}{1400}\gamma^2 + O(\gamma^3) \right], \tag{4.24}$$

$$\zeta = a \left[ S^2 + \frac{1}{300}(a_{20}S^2 + \sum_{j=1}^3 a_{2j}S^{2j}T^2)\gamma + \frac{1}{22050000} \left( a_{40}S^2 + \sum_{j=1}^6 a_{4j}S^{2j}T^2 \right) \gamma^2 + O(\gamma^3) \right]. \tag{4.25}$$

### High-order long wave approximation

When the solitary wave amplitude is defined by  $a_s = \zeta(0)$ , its relationship with  $a$  can be expanded, in terms of  $\gamma$ , as

$$a_s = a \left[ 1 + \frac{a_{20}}{300} \gamma + \frac{a_{40}}{22050000} \gamma^2 + O(\gamma^3) \right], \quad (4.26)$$

which can be inverted to

$$a = a_s \left[ 1 - \frac{5 + 6a_s + a_s^2}{20} \gamma_s + \frac{2100 + 10215a_s + 14233a_s^2 + 6941a_s^3 + 823a_s^4}{42000} \gamma_s^2 + O(\gamma_s^3) \right], \quad (4.27)$$

where  $\gamma_s = a_s/(1 + a_s)$  and  $\gamma = \gamma_s - (5 + a_s)\gamma_s^2/20 + O(\gamma_s^3)$ .

Under the small-amplitude assumption of  $\alpha = O(\beta^2)$ , after expanding (4.13) in  $\alpha$ , the third-order solitary wave solution (4.24) and (4.25) can be reduced to the third-order weakly nonlinear solution given by

$$c_s/(gh)^{1/2} = [1 + \frac{1}{2}\alpha_s - \frac{3}{20}\alpha_s^2 + \frac{3}{56}\alpha_s^3 + O(\alpha_s^4)], \quad (4.28a)$$

$$\zeta/h = \alpha_s[S^2 - \frac{3}{4}\alpha_s S^2 T^2 + \alpha_s^2(\frac{5}{8}S^2 T^2 - \frac{101}{80}S^4 T^2) + O(\alpha_s^3)], \quad (4.28b)$$

$$k_s h = (\frac{3}{4})^{1/2} \alpha_s^{1/2} [1 - \frac{5}{8}\alpha_s + \frac{71}{128}\alpha_s^2 + O(\alpha_s^3)], \quad (4.28c)$$

where  $\alpha_s = a_s/h$  and we have made the weakly nonlinear approximation to (4.26) to find  $\alpha_s = \alpha + \alpha^2/4 + \alpha^3/8 + O(\alpha^4)$ , which can be inverted to

$$\alpha = \alpha_s - \frac{1}{4}\alpha_s^2 + O(\alpha_s^4). \quad (4.29)$$

The weakly nonlinear solution given by (4.28) was first obtained by Grimshaw (1971).

#### 4.1.3. Comparison of solutions

Figure 2 shows the comparison between the strongly and weakly nonlinear solitary wave solutions along with the fully nonlinear Euler solutions obtained numerically by Longuet-Higgins & Fenton (1974) for the solitary wave speed  $c$  and its total mass  $M$  defined by

$$M = \int_{-\infty}^{\infty} \zeta(X) dX. \quad (4.30)$$

As shown in figure 2(a), as the order of approximation increases, the strongly nonlinear solution for the wave speed  $c$  approaches the Euler solution and the comparison is reasonable up to  $a_s/h = 0.65$ , where the difference is less than 1%. As shown in figure 2(b), a similar conclusion can be made to the total mass  $M$ , for which the difference is approximately 3% when  $a_s/h = 0.65$ . Considering that the maximum solitary wave amplitude is approximately  $a_s/h = 0.827$ , the third-order solitary wave solution can be considered a good approximation to the Euler solution for finite-amplitude solitary waves. The difference increases with the wave amplitude, but this is not so surprising. The solitary wave becomes sharper near the crest as the amplitude increases so that the long wave approximation starts to be locally invalid.

In figure 3, the strongly nonlinear solitary wave profiles for  $a_s/h = 0.460$  are compared with the Euler solutions computed by Li *et al.* (2004). While the first-order solution (or Rayleigh's solution) is wider than the Euler solution, both the second-order and

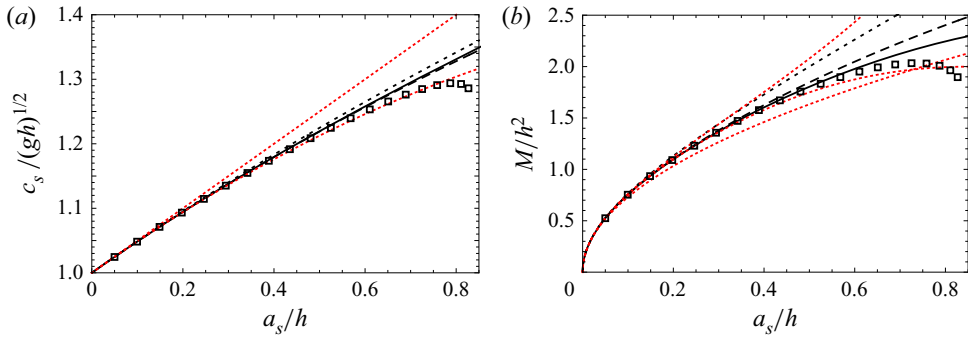


Figure 2. (a) Solitary wave speed  $c$  and (b) total mass  $M$  vs amplitude  $a_s$  for different orders of approximation (dotted: first order; dashed: second order; solid: third order). The black and red lines represent the strongly nonlinear and weakly nonlinear solutions, respectively. The symbols are the numerical solution of the Euler equations from Longuet-Higgins & Fenton (1974). In (a), the third-order weakly nonlinear solution for  $c$  is close to the third-order strongly nonlinear solution and is not shown here.

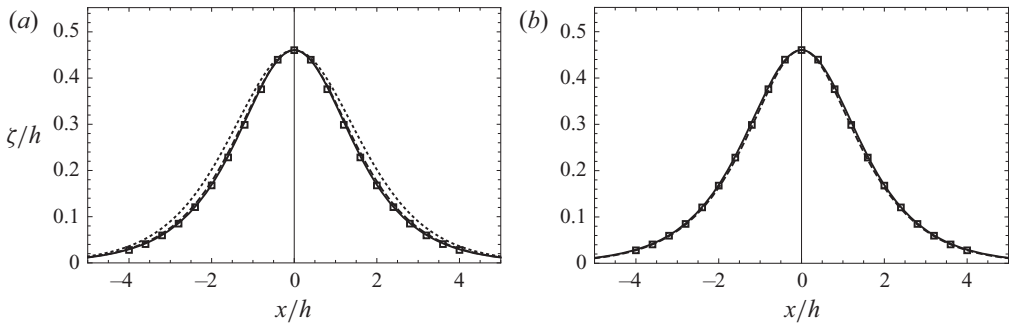


Figure 3. Solitary wave profiles for  $a_s/h = 0.460$ . (a) Strongly nonlinear solutions under the first- (dotted), second- (dashed) and third-order (solid) approximations are compared with the numerical solution of the Euler equations (symbols) computed by Li, Hyman & Choi (2004). (b) Comparison between the strongly (solid) and weakly (dashed) nonlinear solutions under the third-order approximation. The first- and second-order weakly nonlinear solutions compare poorly with the Euler solutions and are not shown here.

third-order solutions agree well with the Euler solution. While the first- and second-order weakly nonlinear solutions (not shown here) compare poorly with the Euler solution, the third-order weakly nonlinear solution is as good as the third-order strongly nonlinear solution.

In figure 4, the wave amplitude is further increased to  $a_s/h = 0.663$ . As can be seen in figure 4(a), the comparison of the strongly nonlinear solution with the Euler solution improves as the order of approximation increases. The third-order strongly nonlinear solution is slightly wider than the Euler solution, in particular near the crest, where short-wavelength components are no longer negligible. Away from the crest, the third-order solution agrees well with the Euler solution.

In figure 4(b), it is surprising to see that the third-order weakly nonlinear solution compares better with the Euler solution than the strongly nonlinear one, in particular near the crest, even though the amplitude ( $a_s/h = 0.663$ ) is too large for the weakly nonlinear theory to be valid. Furthermore, the long wave theory is expected to fail to describe the profile near crest when the wave amplitude is large as the wave slope becomes so steep (eventually to form a corner at the maximum amplitude). As discussed in Murashige &



## High-order long wave approximation

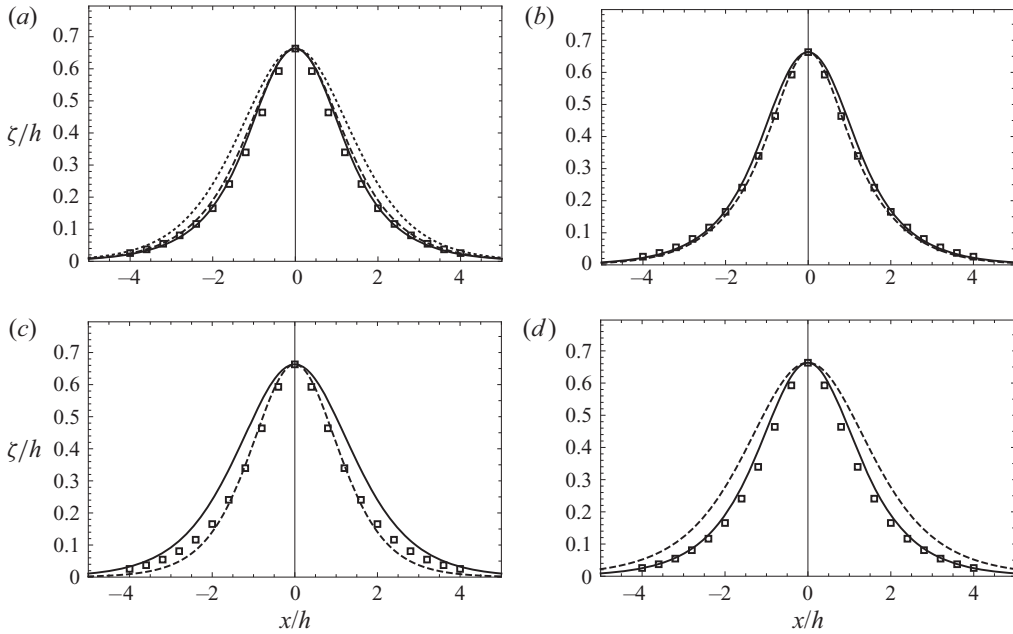


Figure 4. Solitary wave profiles for  $a_s/h = 0.663$ . In (a), strongly nonlinear solutions under the first- (dotted), second- (dashed) and third-order (solid) approximations are compared with the numerical solution of the Euler equations (symbols) computed by Li *et al.* (2004). In (b–d), the strongly nonlinear solutions (solid) are compared with the weakly nonlinear solutions (dashed) under the third-, first-, second-order approximations, respectively. Notice that the comparison of the weakly nonlinear solution with the Euler solution (symbols) depends sensitively on the order of approximation.

Choi (2015) in terms of singularity structures in the complex planes of different theoretical models, this agreement might be coincident. As can be seen in figure 2, the comparison of the weakly nonlinear solution with the Euler solution depends sensitively on the order of nonlinearity while that of the strongly nonlinear solution improves uniformly with the order. In addition, the strongly nonlinear solution better behaves on the outskirts of the solitary wave, where the long wave approximation should be applicable. This can be also seen in figure 4(c,d), where the Euler solution is compared with first- and second-order solutions. The weakly nonlinear solution near the crest agrees well with the Euler solution under the first-order approximation, but compares poorly under the second-order approximation. On the other hand, irrespective of the order of approximation, the strongly nonlinear solitary wave solution (4.25) shows uniform convergence to the Euler solution and can be used reliably. Furthermore, as shown later in figure 5, the weakly nonlinear solutions for finite-amplitude waves are no longer valid when their velocity profiles are compared with the Euler solutions.

### 4.2. Velocity and pressure fields induced by a solitary wave

The velocity and pressure fields induced by a solitary wave is of great interest for applications. After the  $M$ th-order solitary wave solution is found, one should find the corresponding velocity and pressure fields with care so that their expressions are asymptotically consistent with the solitary wave solution. Otherwise, the results contain higher-order terms that have been neglected for the solitary wave solution and could show poor agreement with the Euler solutions.

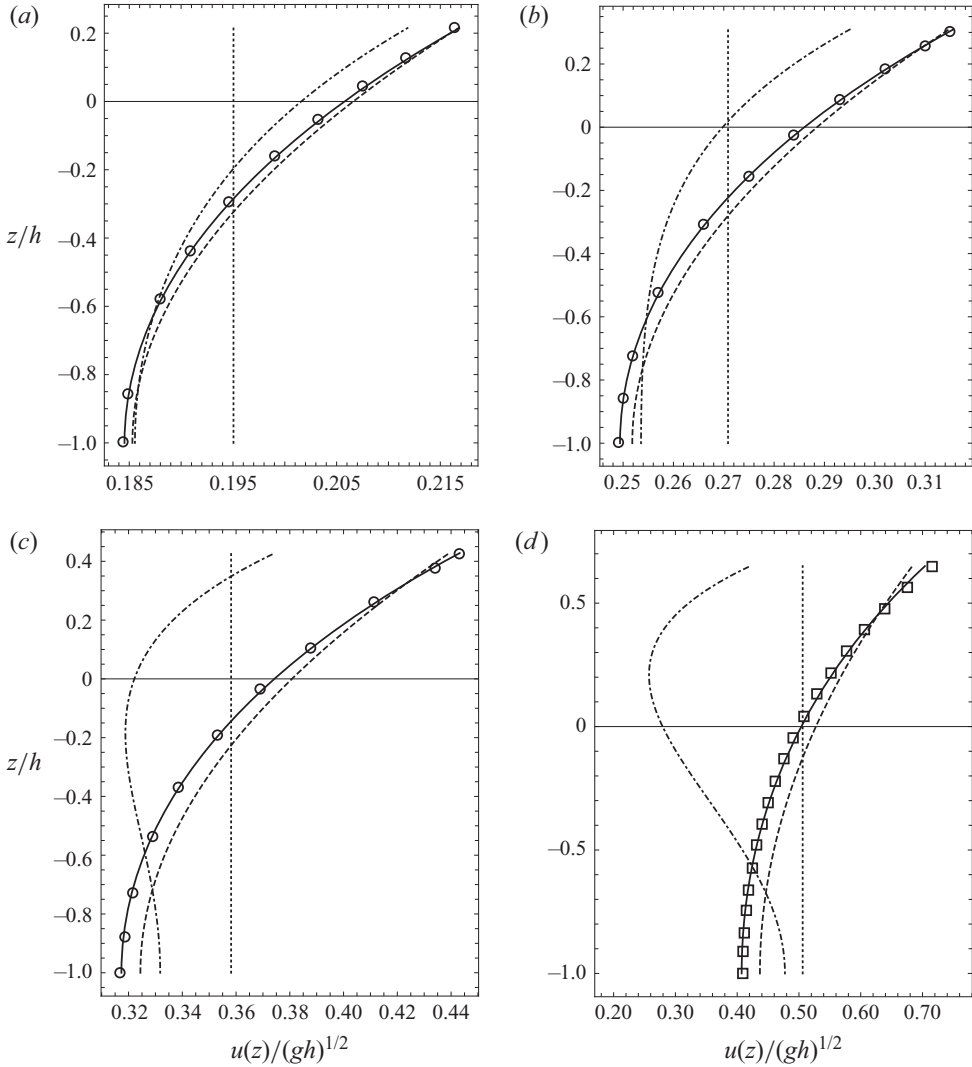


Figure 5. Horizontal velocity profile  $U(z)$  below the crest of a solitary wave for (a)  $a_s/h = 0.215$ ; (b)  $a_s/h = 0.310$ ; (c)  $a_s/h = 0.428$ ; (d)  $a_s/h = 0.65$ . The third-order solution (solid) is compared with the second-order solution (dashed), the third-order weakly nonlinear solution (dot-dashed) given by (4.38), the numerical solution of the level-4 GN model of Zhao *et al.* (2014) (circles) and the numerical solution of Tanaka (1986) shown in Madsen *et al.* (2002) (squares). Notice that the first-order solution (dotted) is independent of  $z$ .

#### 4.2.1. Velocity fields

The horizontal and vertical velocities,  $(u, w) = (\phi_X, \phi_z)$ , induced by a solitary wave can be computed, from (2.26), as

$$u(X, z) = \sum_{m=0}^{\infty} \frac{(-1)^m}{(2m)!} (z+h)^{2m} D^{2m} v, \tag{4.31}$$

$$w(X, z) = \sum_{m=0}^{\infty} \frac{(-1)^{m+1}}{(2m+1)!} (z+h)^{2m+1} D^{2m+1} v, \tag{4.32}$$

*High-order long wave approximation*

where  $-h \leq z \leq \zeta$ . To find an asymptotically consistent velocity field, the bottom velocity  $v(X) = D\phi_b$  should be first expanded as

$$v = \sum_{m=0}^{\infty} v_{2m}^s, \tag{4.33}$$

where  $v_{2m}^s = O(\beta^{2m})$  can be found by substituting into (4.2) the expansions for  $\zeta$  and  $c$  given by (4.14). For example, up to the third order,  $v_{2m}^s$  ( $m = 0, 1, 2$ ) can be explicitly found as

$$v_0^s = \frac{c_0 \zeta_0}{\eta_0}, \tag{4.34a}$$

$$v_2^s = \frac{c_2 \zeta_0}{\eta_0} + \frac{c_0 h}{6\eta_0^2} [6\zeta_2 + \eta_0(-2\zeta_0'^2 + \eta_0 \zeta_0'')], \tag{4.34b}$$

$$\begin{aligned} v_4^s = & \frac{c_4 \zeta_0}{\eta_0} + \frac{c_2 h}{6\eta_0^2} [6\zeta_2 + \eta_0(-2\zeta_0'^2 + \eta_0 \zeta_0'')] \\ & + \frac{c_0 h}{360\eta_0^3} [360\eta_0 \zeta_4 - 360\zeta_2^2 + 120\eta_0 \zeta_0'^2 \zeta_2 - 240\eta_0^2 \zeta_0' \zeta_2' + 60\eta_0^3 \zeta_2'' \\ & + \eta_0^2 (32 \zeta_0'^4 - 8\eta_0 \zeta_0'^2 \zeta_0'' - 22\eta_0^2 \zeta_0''^2 - 16\eta_0^2 \zeta_0' \zeta_0''' + 7\eta_0^3 \zeta_0'''')], \end{aligned} \tag{4.34c}$$

where the expressions for  $\zeta_{2m}$  and  $c_{2m}$  have been obtained in § 4.1. Then, after substituting (4.33) into (4.31) and (4.32), one can find the following expressions for  $u$  and  $w$

$$u(X, z) = \sum_{m=0}^{\infty} u_{2m}^s(X, z), \quad u_{2m}^s = \sum_{j=0}^m \frac{(-1)^j}{(2j)!} (z+h)^{2j} D^{2j} v_{2(m-j)}^s, \tag{4.35a,b}$$

$$w(X, z) = \sum_{m=0}^{\infty} w_{2m}^s(X, z), \quad w_{2m}^s = \sum_{j=0}^m \frac{(-1)^{j+1}}{(2j+1)!} (z+h)^{2j+1} D^{2j+1} v_{2(m-j)}^s, \tag{4.36a,b}$$

where  $u_{2m}^s$  and  $w_{2m}^s$  are both  $O(\beta^{2m})$ . The horizontal velocity profile below the solitary wave crest is also of interest and can be found as  $U(z) = u(0, z)$  as

$$\begin{aligned} U(z)/(gh)^{1/2} = & \frac{\alpha}{(1+\alpha)^{1/2}} \left[ 1 + \left\{ -\frac{\alpha}{10} + \frac{3}{4} \frac{(1+z/h)^2}{1+\alpha} \right\} \gamma \right. \\ & + \left\{ -\frac{\alpha(5820 + 8519\alpha + 3194\alpha^2)}{21000} + \frac{3\alpha(1+6\alpha)}{40} \frac{(1+z/h)^2}{1+\alpha} \right. \\ & \left. \left. + \frac{3(2-\alpha)}{16} \frac{(1+z/h)^4}{(1+\alpha)^2} \right\} \gamma^2 + O(\gamma^3) \right], \end{aligned} \tag{4.37}$$

from which the horizontal velocity at the crest  $U_c$  can be obtained as  $U_c = U(a_s)$ .

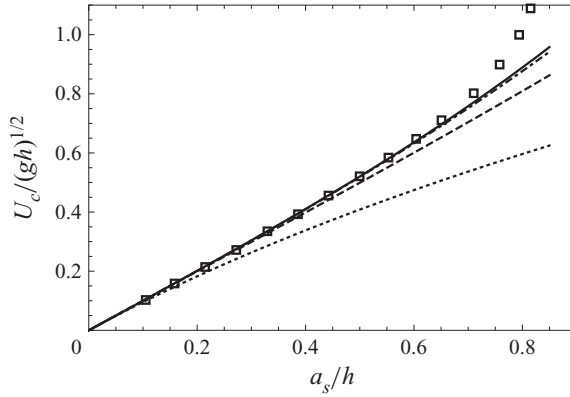


Figure 6. The particle velocity at the crest  $U_c$  vs the solitary wave amplitude  $a_s$ . The first (dotted), second (dashed) and third-order (solid) strongly nonlinear solutions are compared with the numerical solution of the Euler equations of Tanaka (1986) (symbols) as well as the third-order weakly nonlinear solution (dot-dashed).

By expanding (4.37) for small  $\alpha_s$ , the weakly nonlinear solution correct to the third order in  $\alpha_s$  can be obtained as

$$\begin{aligned}
 U(z)/(gh)^{1/2} &= \alpha_s + \frac{3}{4}\alpha_s^2[-1 + (1 + z/h)^2] \\
 &+ \alpha_s^3[\frac{21}{40} - \frac{9}{4}(1 + z/h)^2 + \frac{3}{8}(1 + z/h)^4] + O(\alpha_s^4).
 \end{aligned}
 \tag{4.38}$$

The horizontal velocity at the crest  $U_c = U(a_s)$  is given, after neglecting terms of  $O(\alpha_s^4)$ , by

$$U_c/(gh)^{1/2} = \alpha_s + \frac{3}{20}\alpha_s^3 + O(\alpha_s^4).
 \tag{4.39}$$

These third-order weakly nonlinear solutions given by (4.38) and (4.39) are identical to those in Grimshaw (1971).

In figure 5, the vertical profile of the horizontal velocity below the solitary wave crest  $U(z)$  is computed for  $a_s/h = 0.65$  and is compared with the numerical solution of the Euler equations of Tanaka (1986), which was also confirmed by Madsen *et al.* (2002). Once again, the third-order strongly nonlinear solution for the horizontal velocity profile shows good agreement with the Euler solution. It is interesting to notice that there is a considerable discrepancy between the third-order weakly nonlinear solution given by (4.38) and the Euler solution for the velocity profile although the two solutions agree well for the wave profile. This shows that an asymptotic result should be used with care, in particular, when it is applied to a parameter range outside its validity. Figure 6 shows the horizontal velocity at the crest of the solitary wave  $U_c$  vs  $a_s$ . Compared with the first-order solution (Rayleigh’s solution), the third-order solution shows considerable improvement in the comparison with the Euler solution of Tanaka (1986).

#### 4.2.2. Pressure field

Using the Bernoulli equation given by

$$p = -\rho \left[ gz + \frac{\partial \phi}{\partial t} + \frac{1}{2}(u^2 + w^2) \right],
 \tag{4.40}$$

the pressure field  $p(x, z, t)$  can be found as

$$p(x, z, t) = -\rho gz + \sum_{m=0}^{\infty} p_{2m}(\phi_b, z), \quad (4.41)$$

where  $p_{2m}$  are given, from (2.6a) and (4.35) and (4.36), by

$$\begin{aligned} p_{2m} = & \rho(-1)^{m+1}(z+h)^{2m} \left[ \frac{1}{(2m)!} \frac{\partial}{\partial t} (D^{2m-1}v) \right. \\ & + \frac{1}{2} \sum_{l=0}^m \left\{ \frac{1}{(2l)!(2(m-l))!} (D^{2l}v)(D^{2(m-l)}v) \right. \\ & \left. \left. + \frac{(z+h)^2}{(2l+1)!(2(m-l)+1)!} (D^{2l+1}v)(D^{2(m-l)+1}v) \right\} \right]. \quad (4.42) \end{aligned}$$

In a frame of reference moving with a solitary wave, the dynamic bottom pressure defined by  $P(X) = p(X, -h) - \rho gh$  is given, from (4.40), by

$$P(X) = p_0(\phi_b, -h) = \rho(cv - \frac{1}{2}v^2), \quad (4.43)$$

which can be also found from (4.41) with  $p_{2m} = 0$  at  $z = -h$  for  $m \neq 0$ . To compute the dynamic bottom pressure, the expansion for  $v$  given by (4.33) is substituted into (4.43) and is re-arranged to have

$$P(X) = \sum_{m=0}^{\infty} P_{2m}^s(X), \quad P_{2m}^s(X) = \rho \sum_{j=0}^m \left( c_{2m} v_{2(m-j)}^s - \frac{1}{2} v_{2m}^s v_{2(m-j)}^s \right). \quad (4.44a,b)$$

In particular, to the third order in  $\gamma$ , the bottom pressure below the crest of the solitary wave  $P_c = P(0)$  is given by

$$\frac{P_c}{\rho gh} = \frac{2+\alpha}{2} \gamma + \frac{\alpha^2}{10} \gamma^2 - \frac{\alpha}{10500} (2610 + 3907\alpha + 1597\alpha^2) \gamma^3 + O(\gamma^4). \quad (4.45)$$

Under the weakly nonlinear assumption, the expression of  $P_c$  in (4.45) can be reduced to

$$\frac{P_c}{\rho gh} = \alpha_s - \frac{3}{4}\alpha_s^2 + \frac{3}{4}\alpha_s^3 + O(\alpha_s^4), \quad (4.46)$$

where (4.29) has been used for the expression of  $\alpha_s$  in terms of  $\alpha$ . This third-order weakly nonlinear result was found previously by Fenton (1972).

Figure 7 shows the variation of the bottom pressure  $P_c$  with the wave amplitude  $a_s$ . Compared with the third-order strongly nonlinear solution given by (4.45), the lower-order solutions as well as the third-order weakly nonlinear solution over-predicts the bottom pressure  $P_c$  when the wave amplitude is finite.

### 5. Truncated evolution equations for long waves

The infinite series on the right-hand sides of the system given by (3.3) need to be truncated for numerical computations. The nonlinear evolution equations for  $\zeta$  and  $\phi_b$  correct to

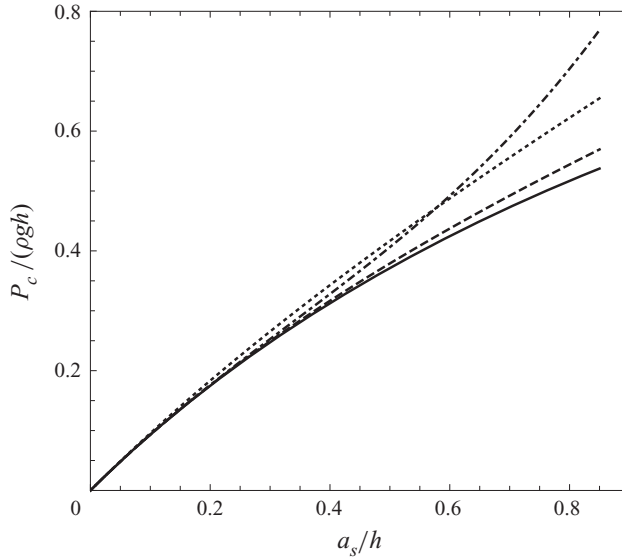


Figure 7. Bottom pressure below the wave crest  $P_c$  vs the solitary wave amplitude  $a_s$ . The third-order solution (solid) is compared with the first- (dotted) and second-order (dashed) solutions as well as the third-order weakly nonlinear solution (dot-dashed) of Grimshaw (1971).

$O(\beta^{2M})$  are then given by

$$\zeta_t = \sum_{m=0}^M Q_{2m}(\zeta, \phi_b), \quad \Phi_t = \sum_{m=0}^M R_{2m}(\zeta, \phi_b), \quad \Phi = \sum_{m=0}^M \Phi_{2m}(\zeta, \phi_b), \quad (5.1a-c)$$

where  $\Phi_{2m}$ ,  $Q_{2m}$  and  $R_{2m}$  are given by (3.1), (3.4) and (3.5), respectively. This system will be referred to as the  $M$ th-order system.

Under the small-amplitude assumption of  $\zeta/h = O(a/h) \ll 1$ , the truncated system (5.1) can be linearized to

$$\zeta_t = \mathcal{S}_{2M}[\phi_b], \quad \mathcal{C}_{2M}[\phi_{b_t}] = -g\zeta, \quad (5.2a,b)$$

where the linear operators  $\mathcal{S}_{2M}$  and  $\mathcal{C}_{2M}$  are given by

$$\mathcal{S}_{2M} = \sum_{m=0}^M \frac{(-1)^{m+1}}{(2m+1)!} h^{2m+1} \nabla^{2(m+1)}, \quad \mathcal{C}_{2M} = \sum_{m=1}^M \frac{(-1)^m}{(2m)!} h^{2m} \nabla^{2m}. \quad (5.3a,b)$$

Notice that  $\mathcal{C}_{2M}[\phi_b]$  and  $\mathcal{S}_{2M}[\phi_b]$  are the linear approximations to  $\Phi$  and  $W$ . The linear dispersion relation for (5.2) is then given by (2.16), which shows that the wave frequency is always real for any choice of  $k$  and  $M$ .

When the zeroth-order ( $M = 0$ ) approximation is made to (5.1), we have

$$\zeta_t + \nabla \cdot (\eta \nabla \phi_b) = 0, \quad \phi_{b_t} + g\zeta + \frac{1}{2} |\nabla \phi_b|^2 = 0, \quad (5.4a,b)$$

which is the system of (non-dispersive) shallow water equations.

## High-order long wave approximation

### 5.1. First-order model

When the leading-order dispersive terms of  $O(\beta^2)$  are included, (5.1) can be reduced to the first-order ( $M = 1$ ) system given by

$$\zeta_t + \nabla \cdot \left[ \left( \eta - \frac{\eta^3}{3!} \nabla^2 \right) \nabla \phi_b \right] = 0, \quad (5.5a)$$

$$\left[ \left( 1 - \frac{\eta^2}{2!} \nabla^2 \right) \phi_b \right]_t + g\zeta + \frac{1}{2} \nabla \phi_b \cdot \nabla \phi_b = \nabla \cdot \left( \frac{\eta^2}{2!} \nabla^2 \phi_b \nabla \phi_b \right), \quad (5.5b)$$

which is the system derived by Wei *et al.* (1995) for the bottom velocity potential. For weakly nonlinear waves of  $\alpha = O(\beta^2)$ , this first-order system can be further reduced to the first-order weakly nonlinear model

$$\zeta_t + \nabla \cdot [(h + \zeta) \nabla \phi_b] - \frac{h^3}{3!} (\nabla^2)^2 \phi_b = 0, \quad (5.6a)$$

$$\left( 1 - \frac{h^2}{2!} \nabla^2 \right) \phi_{bt} + g\zeta + \frac{1}{2} \nabla \phi_b \cdot \nabla \phi_b = 0, \quad (5.6b)$$

which was first obtained by Mei & Le Méhauté (1966).

After taking the gradient, the first-order system (5.5) can be written, in terms of the bottom velocity  $\mathbf{v} = \nabla \phi_b$ , as

$$\zeta_t + \nabla \cdot \left[ \left( \eta - \frac{\eta^3}{3!} \nabla^2 \right) \mathbf{v} \right] = 0, \quad (5.7a)$$

$$\left[ \mathbf{v} - \nabla \left( \frac{\eta^2}{2!} \nabla \cdot \mathbf{v} \right) \right]_t + \nabla \left( g\zeta + \frac{1}{2} \mathbf{v} \cdot \mathbf{v} \right) = \nabla \left[ \nabla \cdot \left\{ \frac{\eta^2}{2!} (\nabla \cdot \mathbf{v}) \mathbf{v} \right\} \right]. \quad (5.7b)$$

This system is asymptotically equivalent to the strongly nonlinear long wave model for the depth-averaged velocity, or the SG/GN equations. Using the relationship between the bottom velocity  $\mathbf{v}$  and the depth-averaged velocity  $\bar{\mathbf{u}}$  given, from (3.11), by

$$\mathbf{v} = \bar{\mathbf{u}} + \frac{\eta^2}{3!} \nabla^2 \bar{\mathbf{u}} + O(\beta^4), \quad (5.8)$$

equation (5.7a) becomes (3.10) while (5.7b) can be written as

$$\left[ \bar{\mathbf{u}} - \frac{1}{\eta} \nabla \left( \frac{\eta^3}{3} \nabla \cdot \bar{\mathbf{u}} \right) \right]_t + \nabla \left( g\zeta + \frac{1}{2} \bar{\mathbf{u}} \cdot \bar{\mathbf{u}} \right) = \nabla \left[ \frac{\eta^2}{2} (\nabla \cdot \bar{\mathbf{u}})^2 + \frac{\bar{\mathbf{u}}}{\eta} \cdot \nabla \left( \frac{\eta^3}{3} \nabla \cdot \bar{\mathbf{u}} \right) \right]. \quad (5.9)$$

Here, we have used  $\nabla(\nabla \cdot \bar{\mathbf{u}}) = \nabla^2 \bar{\mathbf{u}} + O(\beta^2)$ . This scaling can be seen from (3.12), or

$$\nabla \times \bar{\mathbf{u}} = -\frac{1}{3} (\eta \nabla \eta \times \nabla^2 \bar{\mathbf{u}}) + O(\beta^4) = O(\beta^2). \quad (5.10)$$

After rearranging terms and using (5.10), one can show that (5.9) along with (3.10) yields the SG/GN equations for the depth-averaged velocity  $\bar{\mathbf{u}}$

$$\zeta_t + \nabla \cdot (\eta \bar{\mathbf{u}}) = 0, \quad \bar{\mathbf{u}}_t + \bar{\mathbf{u}} \cdot \nabla \bar{\mathbf{u}} + g \nabla \zeta = \frac{1}{\eta} \nabla \left[ \frac{\eta^3}{3} \{ \nabla \cdot \bar{\mathbf{u}}_t + \bar{\mathbf{u}} \cdot \nabla (\nabla \cdot \bar{\mathbf{u}}) - (\nabla \cdot \bar{\mathbf{u}})^2 \} \right]. \quad (5.11a,b)$$

For one-dimensional waves, Rayleigh's solution given by (4.11) is the solitary wave solution of (5.11), as pointed out earlier, with  $\bar{u} = c(\zeta/\eta)$ .

5.2. Second-order model

The second-order ( $M = 2$ ) model correct to  $O(\beta^4)$  can be written explicitly as

$$\zeta_t + \nabla \cdot \left[ \left\{ \eta - \frac{\eta^3}{3!} \nabla^2 + \frac{\eta^5}{5!} (\nabla^2)^2 \right\} \nabla \phi_b \right] = 0, \tag{5.12a}$$

$$\begin{aligned} & \left[ \left\{ 1 - \frac{\eta^2}{2!} \nabla^2 + \frac{\eta^4}{4!} (\nabla^2)^2 \right\} \phi_b \right]_t + g\zeta + \frac{1}{2} \nabla \phi_b \cdot \nabla \phi_b \\ & = \nabla \cdot \left( \frac{\eta^2}{2!} \nabla^2 \phi_b \nabla \phi_b \right) - \nabla \cdot \left[ \frac{\eta^4}{4!} \{ \nabla^2 (\nabla^2 \phi_b \nabla \phi_b) + \nabla (\nabla^2 \phi_b)^2 \} \right]. \end{aligned} \tag{5.12b}$$

The truncated total energy correct to  $O(\beta^4)$  is given by  $E = E_0 + E_2 + E_4$  with  $E_{2m}$  ( $m = 0, 1, 2$ ) defined, from (3.15) and (3.16), by

$$E_0 = \frac{1}{2!} \int (g\zeta^2 + \eta \nabla \phi_b \cdot \nabla \phi_b) \, dx, \tag{5.13a}$$

$$E_2 = \frac{1}{3!} \int \eta^3 [(\nabla^2 \phi_b)^2 - \nabla \phi_b \cdot \nabla^2 \nabla \phi_b] \, dx, \tag{5.13b}$$

$$E_4 = \frac{1}{5!} \int \eta^5 [3\nabla^2 (\nabla \phi_b) \cdot \nabla^2 (\nabla \phi_b) - 4(\nabla^4 \phi_b)(\nabla^2 \phi_b) + \nabla \phi_b \cdot \nabla^4 \nabla \phi_b] \, dx. \tag{5.13c}$$

As mentioned previously, unlike the system for the surface velocity potential and that for the depth-averaged velocity, it can be shown that the system given by (5.12) conserves the truncated total energy only asymptotically. Likewise, the second-order solitary wave solution obtained in § 4 is only the asymptotic solution of the second-order system (5.12).

5.3. Truncated model with the full linear dispersion relation

The truncated system (5.1) for the bottom velocity is always well-posed at any order of approximation, but the linear dispersion relation of a lower-order model is inaccurate, in particular, for short waves. While the system is supposed to correctly describe only long waves, one cannot avoid short waves excited by, for example, numerical errors, nonlinearity and bottom variation. Following Whitham (1974), the truncated system (5.1) can be modified to include the full linear dispersion relation as

$$\zeta_t = -\mathcal{L}[\phi_b] + \left[ \left( \sum_{m=0}^M Q_{2m} \right) - \mathcal{S}_{2M}[\phi_b] \right], \tag{5.14a}$$

$$\left[ \phi_b + \left( \sum_{m=1}^M \Phi_{2m} \right) - \mathcal{C}_{2M}[\phi_b] \right]_t = \sum_{m=0}^M R_{2m}, \tag{5.14b}$$

where the Fourier transform of an integral operator  $\mathcal{L}[\phi_b]$  is defined, from (2.5), as  $\widehat{\mathcal{L}[\phi_b]} = -(k \tanh kh) \hat{\phi}_b$  so that  $W \simeq -\mathcal{L}[\phi_b]$ . Here, the local operators  $\mathcal{S}_{2M}$  and  $\mathcal{C}_{2M}$  defined in (5.3) are introduced to eliminate the truncated linear dispersion relation while  $\mathcal{L}[\phi_b]$  provides the full linear dispersion relation:  $\omega^2 = gk \tanh kh$ . This idea was first proposed by Whitham (1974), who replaced the third-order spatial derivative term in the KdV equation by an integral operator that produces the full linear dispersion relation for uni-directional waves. Nevertheless, it should be remarked that the system given by (5.14)



is asymptotically inconsistent and needs to be carefully tested prior to its application. Furthermore, the high-order nonlinearity in the strongly nonlinear long wave model along with the full dispersive terms could increase the wave steepness (Whitham 1974), which makes computations challenging. Even for ill-posed systems, the (unstable) linear terms can be replaced by the same non-local term to regularize the systems (Choi 2019), but the issues mentioned above cannot be avoided. Therefore, care should be taken in using the regularized strongly nonlinear model (5.14) until the interplay between high-order nonlinearity and full dispersion is fully understood.

### 6. Numerical solutions of the system for the bottom velocity

For one-dimensional waves, after differentiating once with respect to  $x$ , the second-order system (5.12) valid to  $O(\beta^4)$  can be written as

$$\zeta_t + \left( \eta v - \frac{\eta^3}{3!} v_{xx} + \frac{\eta^5}{5!} v_{xxxx} \right)_x = 0, \tag{6.1a}$$

$$\left[ v - \left( \frac{\eta^2}{2!} v_x - \frac{\eta^4}{4!} v_{xxx} \right)_x \right]_t + g\zeta_x + vv_x = \left[ \frac{\eta^2}{2!} vv_x - \frac{\eta^4}{4!} (vv_{xxx} + 5v_x v_{xx}) \right]_{xx}, \tag{6.1b}$$

where  $\eta = h + \zeta$  and  $v = \phi_{b_x}$ . After dropping terms proportional to  $\eta^4$  and  $\eta^5$  in (6.1) that are  $O(\beta^4)$ , one can obtain the first-order system valid to  $O(\beta^2)$  as

$$\zeta_t + \left( \eta v - \frac{\eta^3}{3!} v_{xx} \right)_x = 0, \quad \left[ v - \left( \frac{\eta^2}{2!} v_x \right)_x \right]_t + g\zeta_x + vv_x = \left( \frac{\eta^2}{2!} vv_x \right)_{xx}. \tag{6.2a,b}$$

Finite difference schemes have been widely used to solve long wave models due to their simplicity along with their convenience in inverting an operator that appears in the time derivative on the left-hand side of (6.1b), or (6.2b). To test if finite difference approximations are suitable for the strongly nonlinear system for the bottom velocity, we first consider the first-order system (6.2).

#### 6.1. Finite difference approximation to the linearized first-order system

After all physical variables are non-dimensionalized with respect to  $h$  and  $g$  (or, equivalently,  $h = g = 1$  are chosen), the linearized system for  $\zeta$  and  $v$  given, from (6.2), by

$$\zeta_t + v_x - \frac{1}{6} v_{xxx} = 0, \quad (v - \frac{1}{2} v_{xx})_t + \zeta_x = 0, \tag{6.3a,b}$$

can be approximated, using the second-order central difference scheme in space, as

$$\zeta_t + D_0 v - \frac{1}{6} D_0 D_+ D_- v = 0, \quad (v - \frac{1}{2} D_+ D_- v)_t + D_0 \zeta = 0. \tag{6.4a,b}$$

Here,  $D_+$ ,  $D_-$  and  $D_0$  are the forward, backward and central differences, respectively, so that the finite difference approximations for the first-, second- and third-order derivatives

are given by

$$D_0 v_j = \frac{v_{j+1} - v_{j-1}}{2\Delta x} = v_{xj} + \frac{\Delta x^2}{6} v_{xxxj} + O(\Delta x^4), \tag{6.5a}$$

$$D_+ D_- v_j = \frac{v_{j+1} - 2v_j + v_{j-1}}{\Delta x^2} = v_{xxj} + \frac{\Delta x^2}{12} v_{xxxxj} + O(\Delta x^4), \tag{6.5b}$$

$$D_0 D_+ D_- v_j = \frac{v_{j+2} - 2v_{j+1} + 2v_{j-1} - v_{j-2}}{2\Delta x^3} = v_{xxxj} + \frac{\Delta x^2}{4} v_{xxxxxj} + O(\Delta x^4), \tag{6.5c}$$

where  $\Delta x$  is the grid size and  $v_j = (x_j, t)$  with  $x_j = j\Delta x$ . Notice that the terms proportional to  $\Delta x^2$  in (6.5) represent the leading-order truncation errors associated with the central difference approximation adopted here and can be found by expanding  $v_{j\pm 1}$  and  $v_{j\pm 2}$  for small  $\Delta x$  about  $x = x_j$ .

With these finite difference approximations, the linear system (6.3) is modified to

$$\zeta_t + v_x - \frac{1}{6}(1 - \Delta x^2)v_{xxx} - \frac{\Delta x^2}{24} v_{xxxxx} = O(\Delta x^4), \tag{6.6a}$$

$$\left( v - \frac{1}{2}v_{xx} - \frac{\Delta x^2}{24}v_{xxxx} \right)_t + \zeta_x + \frac{\Delta x^2}{6}\zeta_{xxx} = O(\Delta x^4), \tag{6.6b}$$

whose linear dispersion relation can be obtained as

$$\omega^2 = k^2 \left( 1 - \frac{\Delta x^2}{6}k^2 \right) \left[ 1 + \frac{1}{6}k^2 - \frac{\Delta x^2}{6}k^2 \left( 1 + \frac{1}{4}k^2 \right) \right] / \left( 1 + \frac{1}{2}k^2 - \frac{\Delta x^2}{24}k^4 \right), \tag{6.7}$$

which can be reduced to (2.16) with  $M = 1$  as  $\Delta x \rightarrow 0$ . The question is if the right-hand side of (6.7) is always positive when  $\Delta x$  is small, but non-zero. If not,  $\omega$  is purely imaginary for a certain range of  $k$  and the finite difference scheme would then be unstable to disturbances whose wavenumbers are within the range. Notice that the denominator of (6.7) is always positive for  $0 \leq k \leq k_{max}$ , where  $k_{max}$  is the maximum wavenumber resolved by a finite difference scheme given by  $k_{max} = \pi/\Delta x$ . Then, the sign of the right-hand side of (6.7) follows that of its numerator, from which the range of  $\bar{k} = k\Delta x$  for imaginary  $\omega$  or numerical instability can be approximated by  $2 < \bar{k} < \sqrt{6} \simeq 2.449$  for small  $\Delta x$ . This implies that, when the system given by (6.2) is discretized, the disturbances whose wavenumbers are within this range can be unstable when they are excited. As the growth rate in (6.7) is proportional to  $1/\Delta x$  with  $\bar{k} = O(1)$ , the numerical scheme becomes more unstable when  $\Delta x$  is decreased to obtain a more accurate solution.

It should be recalled that this difficulty arises from the finite difference approximation of high-order spatial derivatives in (6.2) even though the system is well-posed. This discussion can be also applied to the weakly nonlinear model for the bottom variable although its nonlinear behaviour would be different from its strongly nonlinear counterpart.

On the other hand, the first-order or SG/GN equations for the depth-averaged velocity  $\bar{u}$  is given, from (A10) after dropping terms of  $O(\beta^4)$ , by

$$\zeta_t + (\eta\bar{u})_x = 0, \quad \left[ \bar{u} - \frac{1}{3\eta}(\eta^3\bar{u}_x)_x \right]_t + g\zeta_x + \bar{u}\bar{u}_x = \left[ \frac{\eta^2}{2}\bar{u}_x^2 + \frac{\bar{u}}{\eta} \left( \frac{\eta^3}{3}\bar{u}_x \right)_x \right]_x. \tag{6.8a,b}$$

### High-order long wave approximation

When the SG/GN equations are linearized and discretized using the previous second-order finite difference scheme, they can be modified to

$$\zeta_t + \bar{u}_x + \frac{\Delta x^2}{6} \bar{u}_{xxx} = O(\Delta x^4), \quad (6.9a)$$

$$\left( \bar{u} - \frac{1}{3} \bar{u}_{xx} - \frac{\Delta x^2}{36} \bar{u}_{xxxx} \right)_t + \zeta_x + \frac{\Delta x^2}{6} \zeta_{xxx} = O(\Delta x^4), \quad (6.9b)$$

whose dispersion relation can be found as

$$\omega^2 = k^2 \left( 1 - \frac{\Delta x^2}{6} k^2 \right)^2 / \left( 1 + \frac{1}{3} k^2 - \frac{\Delta x^2}{36} k^4 \right). \quad (6.10)$$

The right-hand side of (6.10) can be shown always positive for  $0 < k < k_{max}$  for any choice of  $\Delta x$  and, unlike that for the bottom velocity  $v$ , the modified system for the depth-averaged velocity  $\bar{u}$  is always neutrally stable with the second-order central difference approximation. Furthermore, unlike that given by (6.7), the frequency  $\omega$  given by (6.10) for the depth-averaged system is independent of  $\Delta x$  and is bounded as  $\Delta x \rightarrow 0$ , which implies the system given by (6.8) imposes little constraint on the choice of  $\Delta t$  for numerical stability. Therefore, the system for the depth-averaged velocity is more suitable for numerical computations than that for the bottom variable. Unfortunately, the issue of the depth-averaged system is that it could be ill-posed when truncated at even orders in  $\beta^2$ .

While we only consider the first-order system, the similar numerical issues discussed previously are expected to appear in the higher-order systems for the bottom velocity. As the order of approximation increases, we need to include higher-order spatial derivatives, which would make the corresponding modified system more unstable. This indicates that finite difference approximations might not be so suitable to solve the strongly nonlinear system for the bottom velocity given by (6.1) or (6.2). Therefore, we adopt a pseudo-spectral method, with which high-order spatial derivatives can be accurately evaluated.

#### 6.2. Pseudo-spectral method for the second-order system

To solve (6.1), we use a pseudo-spectral method based on Fourier series, where  $\zeta$  and  $v$  are approximated by finite complex Fourier series

$$\zeta(x, t) = \sum_{n=-N/2+1}^{N/2} \hat{\zeta}_n(t) e^{ik_n x}, \quad v(x, t) = \sum_{n=-N/2+1}^{N/2} \hat{v}_n(t) e^{ik_n x}, \quad (6.11a,b)$$

where  $N$  is the total number of Fourier modes for computations and  $k_n = 2\pi n/L$  with  $L$  being the computational domain length. We use a fast Fourier transform routine to compute the complex Fourier coefficients  $(\hat{\zeta}_n, \hat{v}_n)$  for  $-N/2 + 1 \leq n \leq N/2$  defined by

$$\hat{\zeta}_n(t) = \sum_{j=0}^{N-1} \zeta_j(t) e^{-ik_n x_j}, \quad \hat{v}_n(t) = \sum_{j=0}^{N-1} v_j(t) e^{-ik_n x_j}, \quad (6.12a,b)$$

where  $\zeta_j(t) = \zeta(x_j, t)$  and  $v_j(t) = v(x_j, t)$  with  $x_j = j\Delta x (j = 0, \dots, N-1)$ . When linearized, (6.1) yields a coupled system of ordinary differential equations for  $\hat{\zeta}_n(t)$  and  $\hat{v}_n(t)$ , from which one can find the dispersion relation given by (2.16) with  $M = 2$ .

In solving (6.1), the spatial derivatives are evaluated in Fourier space while the nonlinear terms are computed in physical space. Then, the evolution equations in (6.1) are integrated in time using the fourth-order Runge–Kutta (RK4) scheme.

At every time step when a nonlinear system is solved numerically with finite Fourier series, aliasing errors are introduced and a filter needs to be applied to eliminate them. As the order of nonlinearity  $M_{NL}$  is given by  $M_{NL} = 2M + 2$ , with  $M$  being the order of approximation, one can in principle eliminate the aliasing errors by removing the Fourier coefficients  $\hat{\zeta}_n$  and  $\hat{v}_n$  for  $|n| > [(M_{NL} - 1)/(M_{NL} + 1)](N/2)$  so that we only keep the Fourier modes for  $|n| > [2/(M_{NL} + 1)](N/2)$ . Although the total energy is conserved only asymptotically for (6.1), it is monitored to make sure that the de-aliasing filter produces no significant energy loss.

After solving (6.1a) for  $\zeta$  and (6.1b) for  $\Phi_x$  given by

$$\Phi_x = v - \left( \frac{\eta^2}{2!} v_x - \frac{\eta^4}{4!} v_{xxx} \right)_x, \tag{6.13}$$

one needs to invert (6.13) to find  $v$  at a new time step. A similar inversion step was required to solve the regularized two-layer long wave model for internal waves proposed by Choi, Barros & Jo (2009), for which an iterative scheme was developed for the inversion (Choi, Goulet & Jo 2011). Here, we adopt a similar iterative scheme, which can be written as

$$\left( 1 - \frac{\xi^2}{2!} \partial_x^2 + \frac{\xi^4}{4!} \partial_x^4 \right) v^{(n+1)} = \Phi_x + \left[ \left( \frac{\eta^2}{2!} - \frac{\xi^2}{2!} \right) v_x^{(n)} - \left( \frac{\eta^4}{4!} - \frac{\xi^4}{4!} \right) v_{xxx}^{(n)} \right]_x, \tag{6.14}$$

where  $v^{(n)}$  is the estimate after the  $n$ th iteration step ( $n \geq 0$ ),  $v^{(0)}$  is an initial guess and  $\xi$  is a numerical parameter to accelerate the convergence of this iteration scheme, which is chosen to be  $\xi = \eta_{max}$ , as discussed in Appendix C. After the right-hand side of (6.14) is evaluated in physical space, the linear operator with constant coefficients on the left-hand side can be easily inverted in Fourier space. This iterative scheme is repeated until  $\|v^{(n+1)} - v^{(n)}\|_\infty / \|v^{(n)}\|_\infty < 10^{-14}$  is satisfied, where  $\|v^{(n)}\|_\infty$  denotes the maximum of  $|v_j^{(n)}|$  for  $j = 1, \dots, N$ .

Alternatively, one can use (3.7) to find the following approximate expression for  $v$  in terms of two known functions,  $\eta (= h + \zeta)$  and  $\Phi_x$ ,

$$v \simeq v_0 + v_2 + v_4 = \Phi_x + \left( \frac{\eta^2}{2!} \Phi_{xx} \right)_x - \left[ \frac{\eta^2}{2!} \left( \frac{\eta^2}{2!} \Phi_{xx} \right)_{xx} - \frac{\eta^4}{4!} \Phi_{xxxx} \right]_x. \tag{6.15}$$

As this is the asymptotic inversion of (6.13) with an error of  $O(\beta^6)$ , the numerical inversion with the iterative scheme given by (6.14) is more preferable as  $\beta$  increases. In the meantime, (6.15) is used to find an initial guess for  $v$  to start the iteration in (6.14).

In our computations, the steady solitary wave solution of the Euler equations obtained in § 4 is chosen for the initial condition for  $\zeta$  while the steady form of (6.1a), or

$$\left( 1 - \frac{\eta^2}{3!} \partial_x^2 + \frac{\eta^4}{5!} \partial_x^4 \right) v = \frac{c\xi}{\eta}, \tag{6.16}$$

is used to find the initial condition for  $v$  using an iterative scheme similar to (6.14).

Figure 8 shows the numerical solution of the first-order system (6.2) for the propagation of a solitary wave for two different amplitudes:  $a = 0.2$  and  $0.4$ . Notice that  $a_s = a$  for the first-order solution. The total computational domain is given by  $-200 \leq x \leq 200$  although the solution is shown over  $-50 \leq x \leq 50$ . The number of Fourier modes is

## High-order long wave approximation

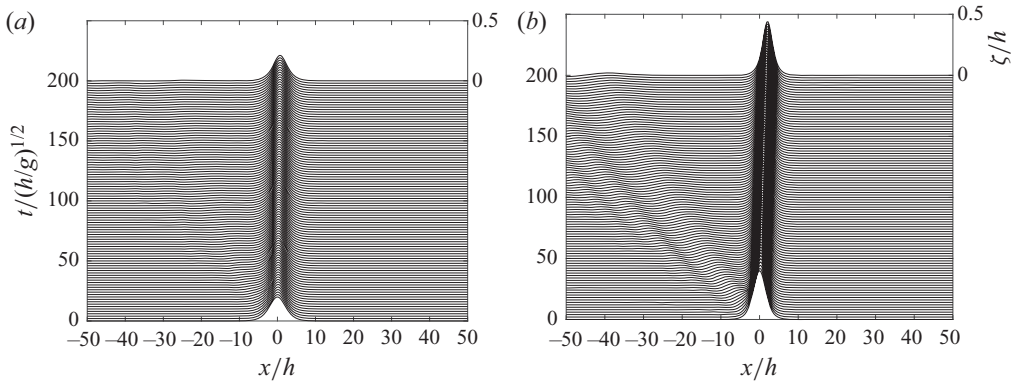


Figure 8. Numerical solutions of the first-order system (6.2) for the propagation of a solitary wave of (a)  $a/h = 0.2$  and (b)  $a/h = 0.4$ . The initial condition for  $\zeta$  is given by the first-order solitary solution (4.11) while that for  $v$  is found by solving numerically (6.16) without the last term on the left-hand side. The time evolution of the surface elevation  $\zeta$  is shown for  $0 \leq t/(g/h)^{1/2} \leq 200$  in a frame of reference moving with the solitary wave speed  $c_0$  defined by (4.10).

$N = (5/2) \times 2^9$  so that  $2^9$  Fourier modes are meaningful after applying the de-aliasing filter. The time step is chosen to be  $\Delta t = 0.1$ , which satisfies the stability condition for the RK4 scheme. At  $t = 200$ , the loss of the truncated total energy  $E = E_0 + E_2 + O(\beta^4)$  defined by (3.16) is approximately 0.199% and 1.703% for  $a = 0.2$  and 0.4, respectively. It should be remembered that the truncated total energy is conserved only asymptotically. As the numerical model runs smoothly, the system for the bottom velocity is confirmed to remain stable when the pseudo-spectral scheme is used. However, as the first-order solitary wave solution of the Euler equations given by (4.11) is not the exact steady solution of the first-order system (6.2), it sheds small-amplitude waves for initial adjustment. For the initial condition for  $v$ , instead of solving numerically (6.16), one can choose  $v_0^s$  given by (4.34a), but the duration for the initial adjustment increases. It is observed that the amplitude of dispersive tails for  $a = 0.4$  is greater than that for  $a = 0.2$ , which implies that the first-order approximation might not be sufficient enough to describe the solitary wave of  $a = 0.4$ .

The numerical solution of the second-order model (6.1) for  $a = 0.4$  is shown in figure 9. In this computation, we use the same numerical parameters as before, except for the number of Fourier modes, which is now  $N = (7/2) \times 2^9$  as the order of nonlinearity increases from 4 to 6. Compared with the first-order solution shown in figure 8(b), the initial solitary wave sheds dispersive tails of smaller amplitudes for a shorter time period and is deformed to an almost steady profile at  $t = 200$ , as can be seen in figure 9(a). The truncated energy  $E = E_0 + E_2 + E_4 + O(\beta^6)$  defined by (3.16) initially decreases in time, but reaches a steady state, as shown in figure 9(b). The total energy loss at  $t = 200$  from its initial value is approximately 0.230%. As shown in figure 9(c), when the numerical solution at  $t = 200$  is compared with the initial condition, it appears slightly ahead of the initial profile. The wave speed computed from the numerical solution of the second-order model increases only by 0.37% from the second-order wave speed  $c_s = 1.197$  computed from (4.24). Therefore, it can be concluded that the second-order model well approximates the second-order solitary wave solution for  $a = 0.4$ . Notice that the solitary wave amplitude  $a_s$  defined by (4.26) for  $a = 0.4$  is given by  $a_s \simeq 0.443$  for the second-order solution.

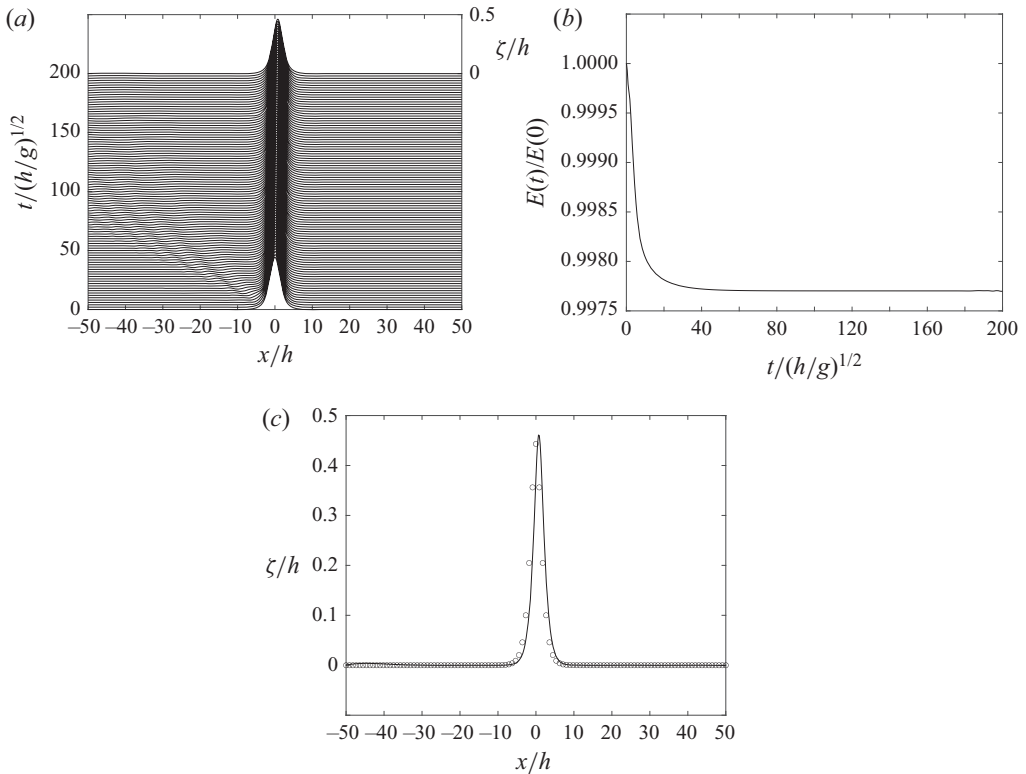


Figure 9. Numerical solution of the second-order system (6.1) initialized with a solitary wave of  $a/h = 0.4$ , or  $a_s/h \simeq 0.443$ . The initial condition for  $\zeta$  is given by the second-order solitary wave solution (4.11) while that for  $v$  is found by solving numerically (6.16). (a) Time evolution of the surface elevation  $\zeta$  is shown for  $0 \leq t(g/h)^{1/2} \leq 200$  in a frame of reference moving with the solitary wave speed  $c = c_0 + c_2$  with  $c_0$  and  $c_2$  defined by (4.10) and (4.18), respectively. (b) Truncated total energy  $E$  vs time  $t$ . (c) Comparison between the numerical solution (solid line) for  $\zeta$  at  $t(g/h)^{1/2} = 200$  and the initial condition (circles).

### 6.3. Comparison with experimental data for head-on collision

To test the second-order model (6.1) for time-dependent problems, we study the head-on collision of two counter-propagating solitary waves for which precision measurements of wave profiles were recently made by Chen & Yeh (2014) using the laser induced fluorescence technique. Although they studied the head-on collision of two solitary waves of the same amplitude ( $a_s = 0.4$ ), their measured wave profile in the first time snapshot shown in Chen & Yeh (2014) is slightly asymmetric about the centre of the two waves and the approximate amplitudes of the right- and left-going waves are found to be approximately  $a_s = 0.40$  and  $a_s = 0.39$ , respectively. As an initial condition, one can locate two solitary waves of these amplitudes far away from each other, but, for the comparison with their experimental data, it is more convenient to place them at the locations where the two solitary waves are observed in the first snapshot.

In figure 10, the first- and second-order solitary wave solutions for  $a_s = 0.4$  are compared with the experimental data of Chen & Yeh (2014) to make sure that the initial solitary wave profile is close to their measurement for this amplitude. The second-order solution given by (4.11) well approximates the measurement and, therefore, the superposition of two second-order solitary wave solutions of slightly different wave amplitudes (0.4 and 0.39) might be considered a good initial condition. Assuming their

### High-order long wave approximation

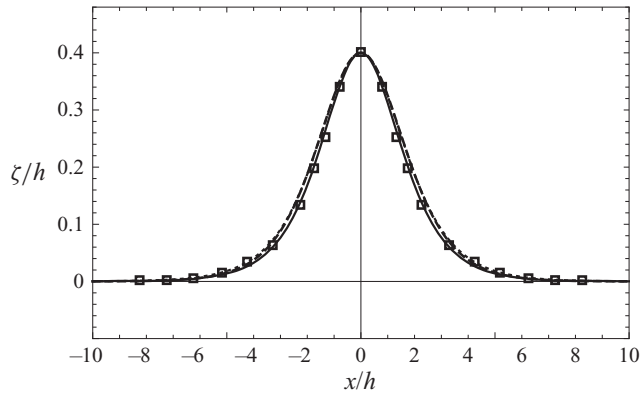


Figure 10. Comparison of solitary wave solutions found in § 4 with the experimental data (symbols) of Chen & Yeh (2014). The second-order solution (solid) is given by  $\zeta = \zeta_0 + \zeta_2$  with for  $a_s/h = 0.4$  ( $a/h = 0.3644$ ), where  $\zeta_0$  and  $\zeta_2$  are given by (4.11) and (4.19), respectively; the first-order solution (dashed) is given by  $\zeta = \zeta_0$  with  $a_s/h = a/h = 0.4$ ; the weakly nonlinear second-order solution (dotted) of Grimshaw (1971) with  $a_s/h = a/h = 0.4$  is also given by (4.28b) without third-order terms. Notice that the first-order solution is almost indistinguishable from the weakly nonlinear second-order solution for this amplitude.

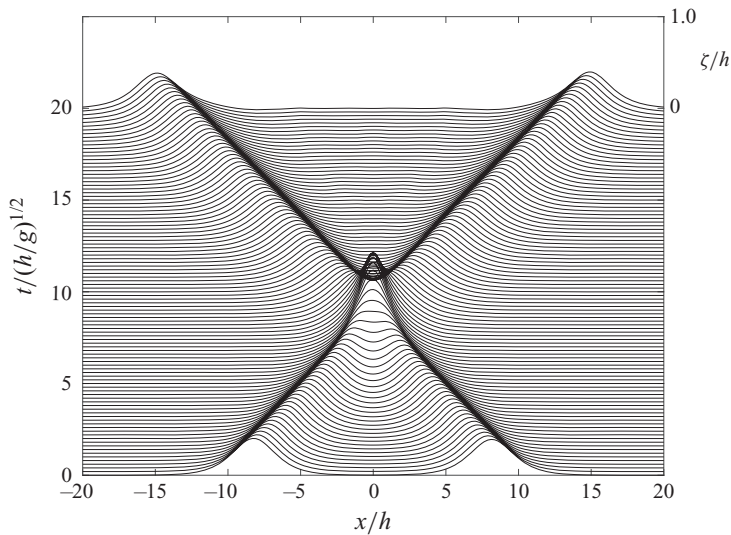


Figure 11. Numerical solution of the second-order system (6.1) for the head-on collision of two solitary waves. The system is initialized with two second-order solitary wave solutions (4.11). The right-going wave of  $a_s/h = 0.4$  ( $a/h \simeq 0.366$ ) is located at  $x/h = -8.23$  while the left-going wave of  $a_s/h = 0.39$  ( $a/h \simeq 0.356$ ) is located at  $x/h = 8.15$ .

interaction is initially small as they are far apart, the two solitary waves located at  $x = -8.23$  and  $8.15$  are linearly superposed at  $t = 0$ . Both the first-order solution given by (4.11) and the weakly nonlinear second-order solution of Grimshaw (1971) given by (4.28b) are also shown in figure 10 and are found slightly wider than the second-order solution (4.11).

The numerical solution of the second-order model (6.1) for the head-on collision of two solitary waves of  $a_s = 0.4$  and  $a_s = 0.39$  is shown in figure 11. The numerical method described in the preceding section is adopted with the following numerical parameters:

$-80 \leq x \leq 80$ ,  $N = (7/2) \times 2^8$ ,  $0 \leq t \leq 20$ ,  $\Delta t = 0.01$ . Notice that the solution over  $-20 \leq x \leq 20$  is presented in [figure 11](#). The numerical filter for de-aliasing is also used and the loss of the truncated energy at  $t = 20$  is approximately 0.130 %.

[Figure 12](#) shows the numerical solution of the second-order model (6.1) compared with the experimental data of [Chen & Yeh \(2014\)](#). In addition, the numerical solutions of two first-order systems: one is the system for the bottom velocity given by (6.2) and the other is the SG/GN equations for the depth-averaged velocity given by (6.8). The aforementioned numerical method for the second-order system is also used for the first-order systems. Notice that the truncated energy is exactly conserved for the SG/GN equations and its loss for the numerical solution is found to be  $1.03 \times 10^{-9}$  %, which implies that our numerical method can be considered accurate. Therefore, one can conclude that the system for the bottom velocity loses more energy due to the fact that the truncated energy is not a conserved quantity, and the de-aliasing filter is not a main source of the energy loss.

In [figure 12](#), the numerical solutions of the first-order models (for both the depth-averaged and bottom velocities) agree reasonably well with the experiments, but they show some discrepancy at the end of collision shown in [figure 12\(e,f\)](#). The measurements at  $t - t_c = 1.02$  and 1.79 are correctly predicted only by the second-order model given by (6.1), which shows that the high-order model is necessary to capture the finite-amplitude effect on the collision.

## 7. Conclusion

We have studied a system for strongly nonlinear long waves expanded in  $\beta^2$ , where the long wave parameter  $\beta = h/\lambda$  is the only small parameter in the expansion without any assumption on the amplitude parameter  $\alpha = a/h$ . It has been shown that, as its linear dispersion relation is always real at any order of approximation in  $\beta^2$ , the high-order long wave model for the bottom velocity is most useful to study the evolution of finite-amplitude waves in shallow water. On the other hand, the long wave systems for other velocities, including the depth-averaged and surface velocities, could be unstable to short-wavelength disturbances at some orders of approximation. For example, the first-order strongly nonlinear system for the surface velocity, or the second-order system for the depth-averaged velocity that could be unstable should be avoided for numerical computations. Furthermore, once a system becomes unstable, its initial value problem is ill-posed, as signified by the unbounded maximum growth rate. It has been shown that the instability and ill posedness are associated with truncation of the linear dispersion relation for long waves.

Using the strongly nonlinear system for the bottom variable, it has been shown that the steady solitary wave solution of the Euler equations can be obtained asymptotically, and an explicit solution valid to the third order in  $\beta^2$  has been obtained. Its validity has been tested for the wave profile, horizontal velocity profile, particle velocity on the crest and bottom pressure. The third-order solution has been found to agree well with numerical solutions of the Euler equations and has improved the first-order strongly nonlinear solution of [Rayleigh \(1876\)](#) and the third-order weakly nonlinear solution previously obtained by [Grimshaw \(1971\)](#).

While the high-order strongly nonlinear system for the bottom velocity is suitable for practical applications, its introduction of high-order spatial derivatives brings another difficulty when it is solved numerically. As finite difference approximations introduce truncation errors in the form of even higher-order spatial derivatives, they alter the behaviour of high wavenumber disturbances of the original system so that the modified system is unstable. To avoid these numerical issues, a pseudo-spectral method with an



High-order long wave approximation

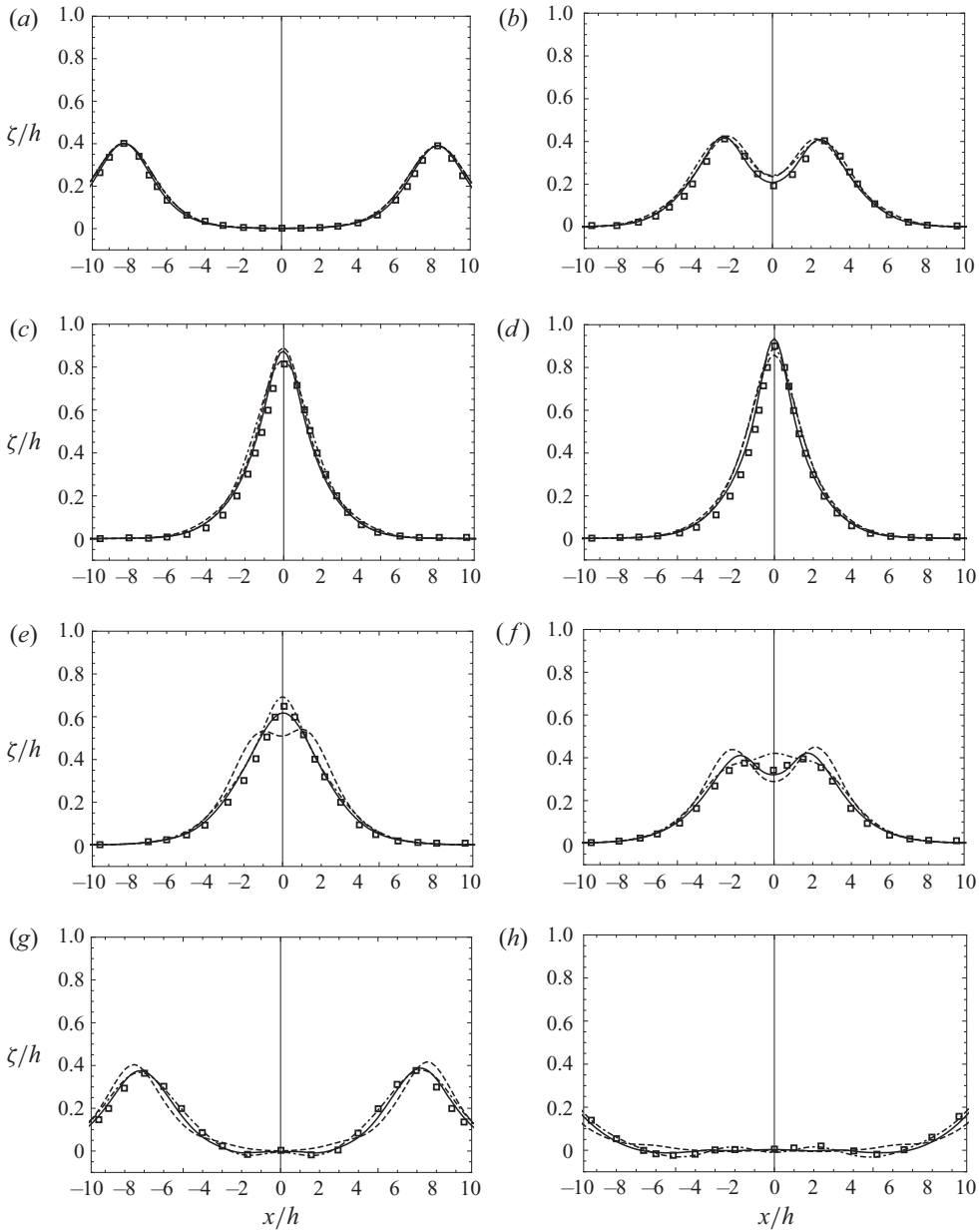


Figure 12. Comparison of numerical solutions (solid: second-order; dashed: first-order; dot-dashed: SG/GN) with the experimental data (symbols) of Chen & Yeh (2014): (a)  $(t - t_c)(g/h)^{1/2} = -7.42$ ; (b)  $-2.69$ ; (c)  $-0.64$ ; (d)  $0$ ; (e)  $1.02$ ; (f)  $1.79$ ; (g)  $6.14$ ; (h)  $10.10$ . Here,  $t_c$  is the time when the maximum peak is observed during the collision.

iterative scheme to invert a non-local operator has been proposed to evaluate accurately high-order spatial derivatives and its effectiveness has been demonstrated for the propagation of a solitary wave and the head-on collision between two counter-propagating solitary waves in comparison with the experimental measurement of Chen & Yeh (2014). A similar numerical technique has been successfully applied to a strongly nonlinear internal

wave model for the velocities at the top and bottom boundaries of a two-layer system (Choi *et al.* 2009), which is a regularized version of the strongly nonlinear long internal wave equations of Miyata (1988) and Choi & Camassa (1999) for the depth-averaged velocities.

To study the evolution of nonlinear long waves, one can use the HOS method discussed in § 2.2, which was originally developed for nonlinear surface waves of arbitrary wavelengths in water of finite depth. As it assumes nothing on the magnitude of  $\beta$ , the HOS method provides the full linear dispersion relation and is therefore free from the ill posedness resulting from the long wave approximation. However, the expansion used in the HOS method is based on the smallness of the wave steepness  $\epsilon$  defined by  $\epsilon = a/\lambda$  with the finite-depth assumption, or  $\beta = h/\lambda = O(1)$ . Therefore, when it is used to study the evolution of long waves, the HOS method implicitly assumes  $\alpha = a/h \ll 1$  as  $\epsilon = \alpha\beta \ll 1$ . For small-amplitude long waves, the low-order HOS method would be acceptable, but, for finite-amplitude long waves, it is not so effective as the strongly nonlinear long wave model (Choi 2019). As the order of nonlinearity is  $2(M + 1)$  in the  $M$ th-order strongly nonlinear long wave model, one should use the  $2(M + 1)$ th-order HOS method to describe the same level of nonlinearity, which would be so computationally expensive. For example, for long waves, the sixth-order HOS model is equivalent to the second-order strongly nonlinear long wave model that we have studied numerically.

The stability of the high-order solitary wave solution found in § 4 is an open question and its investigation is of interest in comparison with that of the fully nonlinear solution of the Euler equations (Tanaka 1986; Tanaka *et al.* 1987). While the strongly nonlinear long wave model has been discussed for the case of flat bottom, it can be generalized, without a major difficulty, to the case when the bottom varies in space and time.

**Funding.** This research was supported by the US National Science Foundation through Grant No. DMS-2108524, and the Brain Pool Program funded by the Ministry of Science and ICT through the National Research Foundation of Korea (Grant No. 2021H1D3A2A01082312).

**Declaration of interests.** The author reports no conflict of interest.

**Author ORCIDs.**

Wooyoung Choi <https://orcid.org/0000-0002-4433-3013>.

### Appendix A. Long wave model for the depth-averaged velocity

From (3.1),  $V = \nabla\Phi$  can be expressed, in terms of  $\zeta$  and  $\mathbf{v} = \nabla\phi_b$ , as

$$V = \sum_{m=0}^{\infty} V_{2m}(\zeta, \mathbf{v}), \quad V_{2m} = \nabla \left[ \frac{(-1)^m}{(2m)!} \eta^{2m} \nabla^{2(m-1)} \nabla \cdot \mathbf{v} \right]. \quad (\text{A1a,b})$$

By substituting (3.11) into (A1),  $V$  can be expressed, in terms of  $\zeta$  and the depth-averaged velocity  $\bar{\mathbf{u}}$ , as

$$V = \sum_{m=0}^{\infty} \bar{V}_{2m}(\zeta, \bar{\mathbf{u}}), \quad (\text{A2})$$

where  $\bar{V}_0 = \bar{\mathbf{u}}$  and  $\bar{V}_{2m}$  ( $m \geq 1$ ) are given by

$$\bar{V}_{2m} = \sum_{j=0}^m \frac{(-1)^j}{(2j)!} \eta^{2j} \nabla^{2j} \bar{\mathbf{v}}_{2(m-j)} + \nabla \eta \sum_{j=0}^{m-1} \frac{(-1)^{j+1}}{(2j+1)!} \eta^{2j+1} \nabla^{2j} \nabla \cdot \bar{\mathbf{v}}_{2(m-j-1)}, \quad (\text{A3})$$

with  $\bar{\mathbf{v}}_{2j}$  defined in (3.11).

*High-order long wave approximation*

Then, the evolution equations for  $\zeta$  and  $\bar{\mathbf{u}}$  can be written as

$$\zeta_t + \nabla \cdot (\eta \bar{\mathbf{u}}) = 0, \quad V_t = \sum_{m=0}^{\infty} \nabla \bar{R}_{2m}(\zeta, \bar{\mathbf{u}}), \quad (\text{A4a,b})$$

where  $V$  is given, in terms of  $\zeta$  and  $\bar{\mathbf{u}}$ , by (A2) with (A3). In (A4),  $\bar{R}_{2m}$  ( $m \geq 0$ ) are given by

$$\bar{R}_0 = -g\zeta - \frac{1}{2} \bar{V}_0 \cdot \bar{V}_0, \quad \bar{R}_2 = -\bar{V}_0 \cdot \bar{V}_2 + \frac{1}{2} \bar{W}_0^2, \quad (\text{A5a,b})$$

$$\begin{aligned} \bar{R}_{2m} = & -\frac{1}{2} \sum_{j=0}^m \bar{V}_{2j} \cdot \bar{V}_{2(m-j)} + \frac{1}{2} \sum_{j=0}^{m-1} \bar{W}_{2j} \bar{W}_{2(m-j-1)} \\ & + \frac{1}{2} |\nabla \zeta|^2 \sum_{j=0}^{m-2} \bar{W}_{2j} \bar{W}_{2(m-j-2)} \quad \text{for } m \geq 2, \end{aligned} \quad (\text{A5c})$$

where  $\bar{W}_{2m}$  are given by

$$\bar{W}_{2m} = \sum_{j=0}^m \frac{(-1)^{j+1}}{(2j+1)!} \eta^{2j+1} \nabla^{2j} \nabla \cdot \bar{\mathbf{v}}_{2(m-j)}. \quad (\text{A6})$$

Although it was presented differently, the system (A4) was previously obtained by Wu (1999) and, from (3.14), its total energy can be expressed, in terms of  $\zeta$  and  $\bar{\mathbf{u}}$ , as

$$E = \frac{1}{2} \int (g\zeta^2 + \eta \bar{\mathbf{u}} \cdot \nabla \Phi) dx = \frac{1}{2} \int \left( g\zeta^2 + \eta \bar{\mathbf{u}} \cdot \sum_{m=0}^{\infty} \bar{V}_{2m} \right) dx. \quad (\text{A7})$$

When truncated at  $O(\beta^2)$ , the system given by (A4) becomes the SG/GN equations while the next-order approximation will yield the second-order system, or the extended SG/GN equations (Matsuno 2016) with  $\bar{V}_{2m}$  and  $\bar{R}_{2m}$  given by

$$\bar{V}_0 = \bar{\mathbf{u}}, \quad \bar{V}_2 = -\frac{\eta^2}{3} \nabla^2 \bar{\mathbf{u}} - \eta \nabla \eta \nabla \cdot \bar{\mathbf{u}}, \quad (\text{A8a,b})$$

$$\bar{V}_4 = \frac{\eta^4}{30} \nabla^4 \bar{\mathbf{u}} - \frac{\eta^2}{18} \nabla^2 (\eta^2 \nabla^2 \bar{\mathbf{u}}) - \frac{\eta^2}{3} |\nabla \eta|^2 \nabla^2 \bar{\mathbf{u}}, \quad (\text{A8c})$$

$$\bar{R}_0 = -g\zeta - \frac{1}{2} \bar{\mathbf{u}} \cdot \bar{\mathbf{u}}, \quad \bar{R}_2 = \frac{\eta^2}{2} (\nabla \cdot \bar{\mathbf{u}})^2 + \bar{\mathbf{u}} \cdot \left( \frac{\eta^2}{3} \nabla^2 \bar{\mathbf{u}} + \eta \nabla \eta \nabla \cdot \bar{\mathbf{u}} \right), \quad (\text{A9a,b})$$

$$\begin{aligned} \bar{R}_4 = & -\bar{\mathbf{u}} \cdot \left[ \frac{\eta^4}{30} \nabla^4 \bar{\mathbf{u}} - \frac{\eta^2}{18} \nabla^2 (\eta^2 \nabla^2 \bar{\mathbf{u}}) - \frac{\eta^2}{3} |\nabla \eta|^2 \nabla^2 \bar{\mathbf{u}} \right] \\ & - \frac{1}{2} \left( \frac{\eta^2}{3} \nabla^2 \bar{\mathbf{u}} + \eta \nabla \eta \nabla \cdot \bar{\mathbf{u}} \right)^2 + \frac{\eta^3}{3} (\nabla \cdot \bar{\mathbf{u}}) (\nabla \eta \cdot \nabla^2 \bar{\mathbf{u}}) + \frac{1}{2} |\nabla \eta|^2 (\eta \nabla \cdot \bar{\mathbf{u}})^2. \end{aligned} \quad (\text{A9c})$$

For one-dimensional waves, the second-order system can be written, in conservative form, as

$$\zeta_t + (\eta\bar{u})_x = 0, \tag{A10a}$$

$$\begin{aligned} & \left[ \bar{u} - \frac{1}{3\eta}(\eta^3\bar{u}_x)_x - \frac{1}{45\eta}(\eta^5\bar{u}_{xx})_{xx} \right]_t + g\zeta_x + \bar{u}\bar{u}_x \\ & = \left[ \frac{\eta^2}{2}\bar{u}_x^2 + \frac{\bar{u}}{\eta} \left( \frac{\eta^3}{3}\bar{u}_x \right)_x - \frac{\eta^4}{18}\bar{u}_{xx}^2 + \frac{\bar{u}}{\eta} \left( \frac{\eta^5}{45}\bar{u}_{xx} \right)_{xx} \right]_x, \end{aligned} \tag{A10b}$$

which conserves exactly the total energy given, from (A7), by

$$E = \frac{1}{2} \int \left( g\zeta^2 + \eta\bar{u}^2 + \frac{\eta^3}{3}\bar{u}_x^2 - \frac{\eta^5}{45}\bar{u}_{xx}^2 \right) dx. \tag{A11}$$

Alternatively, after using (A10a), equation (A10b) can be re-written as

$$\begin{aligned} \bar{u}_t + \bar{u}\bar{u}_x + g\zeta_x &= \frac{1}{3\eta}[\eta^3\{\bar{u}_{xt} + \bar{u}\bar{u}_{xx} - \bar{u}_x^2\}]_x \\ &+ \frac{1}{45\eta}[\{\eta^5(\bar{u}_{xxt} + \bar{u}_x\bar{u}_{xxx} - 5\bar{u}_x\bar{u}_{xx})\}_x - 3\eta^5\bar{u}_{xx}^2]_x, \end{aligned} \tag{A12}$$

which is the form obtained by Matsuno (2015).

### Appendix B. Steady equations for solitary waves

For steady solitary waves, the first four expressions of  $F_{2m}(\zeta; c)$  ( $m = 0, 1, 2, 3$ ) in (4.5) are given by

$$F_0(\zeta; c) = \frac{1}{2}\zeta \left( \frac{2c^2}{\eta} - \frac{c^2\zeta}{\eta^2} - 2g \right), \tag{B1}$$

$$F_2(\zeta; c) = \frac{c^2h^2}{6\eta^2}(\zeta'^2 - 2\eta\zeta''), \tag{B2}$$

$$F_4(\zeta; c) = -\frac{c^2h^2}{90\eta^2}(12\zeta'^4 - 48\eta\zeta''\zeta'^2 + 4\eta^2\zeta'''\zeta' + 2\eta^3\zeta'''' + 3\eta^2\zeta''^2), \tag{B3}$$

$$\begin{aligned} F_6(\zeta; c) &= \frac{c^2h^2}{1890\eta^2}[220\zeta'^6 - 1320\eta\zeta''\zeta'^4 + 156\eta^2\zeta'''\zeta'^3 \\ &+ 3\eta^2\zeta''^2(6\eta\zeta'''' + 145\zeta''^2) - 12\eta^3\zeta'(3\eta\zeta'^5) - 34\zeta'''\zeta''] \\ &- 2\eta^3(2\eta^2\zeta'^6) - 12\eta\zeta''^2 + 3\eta\zeta'''\zeta'' - 65\zeta''^3]. \end{aligned} \tag{B4}$$

**Appendix C. Convergence of the iterative scheme**

Similarly to Choi *et al.* (2011), the convergence of the iterative scheme introduced in (6.14) can be tested as follows. In Fourier space, (6.14) can be written as

$$\left(1 + \frac{\xi^2}{2!}k^2 + \frac{\xi^4}{4!}k^4\right) \hat{v}^{(n+1)} = \widehat{\Phi}_x - \left[ \left(\frac{\eta_0^2}{2!} - \frac{\xi^2}{2!}\right)k^2 + \left(\frac{\eta_0^4}{4!} - \frac{\xi^4}{4!}\right)k^4 \right] \hat{v}^{(n)}, \quad (C1)$$

where  $\eta_0$  is a constant in a possible range of  $\eta$ , which is  $0 < \eta \leq \eta_{max} = 1 + \zeta_{max}$ . After the  $n$ th iteration, the expression for  $\hat{v}^{(n)}$  can be found as

$$\hat{v}^{(n)} = \frac{\widehat{\Phi}_x}{\left(1 + \frac{\xi^2}{2!}k^2 + \frac{\xi^4}{4!}k^4\right)} \left[ \frac{1 - (-r)^n}{1 + r} \right] + (-r)^n \hat{v}^{(0)}, \quad (C2)$$

where  $v^{(0)}$  is the initial guess and  $r$  is given by

$$r = \frac{\left(\frac{\eta_0^2}{2!} - \frac{\xi^2}{2!}\right)k^2 + \left(\frac{\eta_0^4}{4!} - \frac{\xi^4}{4!}\right)k^4}{1 + \frac{\xi^2}{2!}k^2 + \frac{\xi^4}{4!}k^4}. \quad (C3)$$

The behaviour of  $r$  for large  $k$  is of interest (Choi *et al.* 2011). Then, the condition for convergence given by  $|r| < 1$  can be written as

$$\left| \frac{\eta_0^4 - \xi^4}{\xi^4} \right| < 1, \quad (C4)$$

from which one can see that  $|\xi| > 2^{-1/4}\eta_0$ . As  $0 \leq \eta_0 \leq \eta_{max}$ , if the condition of  $|\xi| \geq 2^{-1/4}\eta_{max}$  is satisfied, the iterative scheme always converges. In our computations, we choose  $\xi = \eta_{max}$  for simplicity.

REFERENCES

AGNON, Y., MADSEN, P.A. & SCHÄFFER, H.A. 1999 A new approach to high-order Boussinesq models. *J. Fluid Mech.* **399**, 319–333.  
 CHEN, Y. & YEH, H. 2014 Laboratory experiments on counter-propagating collisions of solitary waves. Part I. Wave interactions. *J. Fluid Mech.* **749**, 577–596.  
 CHOI, W. 2019 On Rayleigh expansion for nonlinear long water waves. *J. Hydrodyn.* **31**, 1115–1126.  
 CHOI, W., BARROS, R. & JO, T.-C. 2009 A regularized model for strongly nonlinear internal solitary waves. *J. Fluid Mech.* **629**, 73–85.  
 CHOI, W. & CAMASSA, R. 1999 Fully nonlinear internal waves in a two-fluid system. *J. Fluid Mech.* **396**, 1–36.  
 CHOI, W., GOULLET, A. & JO, T.-C. 2011 An iterative method to solve a regularized model for strongly nonlinear long internal waves. *J. Comput. Phys.* **230**, 2021–2030.  
 CRAIG, W. & SULEM, C. 1993 Numerical simulation of gravity waves. *J. Comput. Phys.* **108**, 73–83.  
 DOMMERMUTH, D.G. & YUE, D.K.P. 1987 A high-order spectral method for the study of nonlinear gravity waves. *J. Fluid Mech.* **184**, 267–288.  
 FENTON, J. 1972 A ninth-order solution for the solitary wave. *J. Fluid Mech.* **53**, 257–271.  
 GREEN, A.E. & NAGHDI, P.M. 1976 Derivation of equations for wave propagation in water of variable depth. *J. Fluid Mech.* **78**, 237–246.  
 GRIMSHAW, R. 1971 The solitary wave in water of variable depth. Part 2. *J. Fluid Mech.* **46**, 611–622.  
 KIRBY, J.T. 2020 A new instability for Boussinesq-type equations. *J. Fluid Mech.* **894**, F1.  
 LI, Y.A., HYMAN, J.M. & CHOI, W. 2004 A numerical study of the exact evolution equations for surface waves in water of finite depth. *Stud. Appl. Maths* **113**, 303–324.

- LONGUET-HIGGINS, M.S. & FENTON, J.D. 1974 On the mass, momentum, energy and circulation of a solitary wave. *Proc. R. Soc. Lond. A* **340**, 471–493.
- MADSEN, P.A. & AGNON, Y. 2003 Accuracy and convergence of velocity formulations for water waves in the framework of Boussinesq theory. *J. Fluid Mech.* **477**, 285–319.
- MADSEN, P.A., BINGHAM, H.B. & LIU, H. 2002 A new approach to high-order Boussinesq models. *J. Fluid Mech.* **462**, 1–30.
- MADSEN, P.A. & FUHRMAN, D.R. 2020 Trough instabilities in boussinesq formulations for water waves. *J. Fluid Mech.* **889**, A38.
- MADSEN, P.A. & SCHÄFFER, H.A. 1998 Higher-order Boussinesq-type equations for surface gravity waves: derivation and analysis. *Proc. R. Soc. Lond. A* **356**, 3123–3184.
- MATSUNO, Y. 2015 Hamiltonian formulation of the extended Green-Naghdi equations. *Physica D* **301–302**, 1–7.
- MATSUNO, Y. 2016 Hamiltonian structure for two-dimensional extended Green-Naghdi equations. *Proc. R. Soc. A* **472**, 20160127.
- MEI, C.C. & LE MÉHAUTE, B. 1966 Note on the equations of long waves over an uneven bottom. *J. Geophys. Res.* **71**, 393–400.
- MILES, J.W. 1980 Solitary waves. *Annu. Rev. Fluid Mech.* **12**, 11–43.
- MIYATA, M. 1988 Long internal waves of large amplitude. In *Proceedings of the IUTAM Symposium on Nonlinear Water Waves* (ed. H. Horikawa & H. Maruo), pp. 399–406. Springer Verlag.
- MURASHIGE, S. & CHOI, W. 2015 High-order Davies' approximation for a solitary wave solution in Packham's plane. *SIAM J. Appl. Maths* **75**, 189–208.
- NWOGU, O. 1993 An alternative form of the Boussinesq equations for nearshore wave propagation. *ASCE J. Waterway Port Coastal Ocean Engng* **119**, 618–638.
- RAYLEIGH, LORD 1876 On waves. *J. W. S. Phil. Mag.* **1**, 257–279.
- SERRE, F. 1953 Contribution à l'étude des écoulements permanents et variables dans les canaux. *La Houille Blanche* **6**, 830–872.
- SU, C.H. & GARDNER, C.S. 1969 Korteweg-de Vries equation and generalizations. III: derivation of the Korteweg-de Vries equation and Burgers equation. *J. Math. Phys.* **10**, 536–539.
- TANAKA, M. 1986 The stability of solitary waves. *Phys. Fluids* **29**, 650–655.
- TANAKA, M., DOLD, J.W., LEWY, M. & PEREGRINE, D.H. 1987 Instability and breaking of a solitary wave. *J. Fluid Mech.* **185**, 235–248.
- WEI, G., KIRBY, J.T., GRILLI, S.T. & SUBRAMANYA, R. 1995 A fully nonlinear Boussinesq model for surface waves. Part I. Highly nonlinear unsteady waves. *J. Fluid Mech.* **294**, 71–92.
- WEST, B.J., BRUECKNER, K.A., JANDA, R.S., MILDNER, D.M. & MILTON, R.L. 1987 A new numerical method for surface hydrodynamics. *J. Geophys. Res.* **92**, 11803–11824.
- WHITHAM, G.B. 1974 *Linear and Nonlinear Waves*. Wiley.
- WU, T.Y. 1998 Nonlinear waves and solitons in water. *Physica D* **123**, 48–63.
- WU, T.Y. 1999 Modeling nonlinear dispersive water waves. *J. Engng Mech. ASCE* **11**, 747–755.
- ZAKHAROV, V.E. 1968 Stability of periodic waves of finite amplitude on the surface of deep fluid. *J. Appl. Mech. Tech. Phys.* **9**, 190–194.
- ZHAO, B.B., ERTEKIN, R.C., DUAN, W.Y. & HAYATDAVOODI, M. 2014 On the steady solitary-wave solution of the Green-Naghdi equations of different levels. *Wave Motion* **51**, 1382–1395.